Influence of palaeoweathering on trace metal concentrations and environmental proxies in black shales

Journal Item

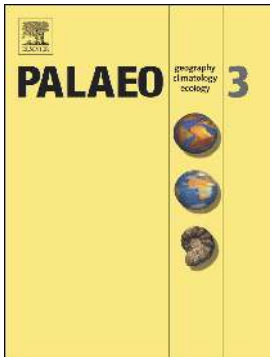

Influence of palaeoweathering on trace metal concentrations and environmental proxies in black shales

Leszek Marynowski, Agnieszka Pisarzowska, Arkadiusz Derkowski, Michał Rakociński, Rafał Szaniawski, Jan Środoń, Anthony S. Cohen

PII: S0031-0182(16)30486-2
DOI: doi: 10.1016/j.palaeo.2017.02.023
Reference: PALAEO 8205

To appear in: *Palaeogeography, Palaeoclimatology, Palaeoecology*

Received date: 18 September 2016
Revised date: 10 February 2017
Accepted date: 11 February 2017

Please cite this article as: Leszek Marynowski, Agnieszka Pisarzowska, Arkadiusz Derkowski, Michał Rakociński, Rafał Szaniawski, Jan Środoń, Anthony S. Cohen , Influence of palaeoweathering on trace metal concentrations and environmental proxies in black shales. The address for the corresponding author was captured as affiliation for all authors. Please check if appropriate. Palaeo(2017), doi: 10.1016/j.palaeo.2017.02.023

Influence of palaeoweathering on trace metal concentrations and environmental proxies in black shales

Leszek Marynowski[1*], Agnieszka Pisarzowska[2], Arkadiusz Derkowski[2], Michał Rakociński[1], Rafał Szaniawski[3], Jan Środoń[2], Anthony S. Cohen[4]

[1] Faculty of Earth Sciences, University of Silesia, Będzińska 60, 41-200 Sosnowiec, Poland

[2] Institute of Geological Sciences, Polish Academy of Sciences – Research Centre in Kraków, ul. Senacka 1, 31-002 Kraków, Poland

[3] Institute of Geophysics, Polish Academy of Science, Ks. Janusza 64, 01-452 Warszawa,, Poland

[4] Department of Environment, Earth and Ecosystems, Centre for Earth, Planetary, Space and Astronomical Research, The Open University, Milton Keynes, MK7 6AA, UK

[*] - corresponding autor; e-mail: leszek.marynowski@us.edu.pl

Abstract

The mineralogical and chemical compositions of Lower Carboniferous (Tournaisian) marine black shale from the Kowala quarry, the Holy Cross Mountains, Poland were investigated. This study focuses on disturbances in palaeoenvironmental proxies caused by palaeoweathering, which progressively changed the major and trace element abundances. Palaeomagnetic investigations reveal that the Devonian – Carboniferous succession was weathered during the Permian-Triassic by the infiltration of oxidizing fluids related to karstification following post-Variscan exhumation. The weathering process led to vermiculitization of chlorite, partial dissolution of calcite and replacement of pyrite by hematite and goethite. Moreover, the concentrations of some trace metals, including Co, Cu, Pb, Mo, Ni, As and U, significantly decreased. Consequently, some elemental abundance ratios that are used as environmental proxies, including U/Th, Ni/Co and V/Cr, were altered. Elements that are bound to iron sulphides (e.g., Mo) appear to be especially prone to mobilization by even a lightly weathered black shale. The documented weathering, including changes in elemental concentrations, can create misinterpretations of the original palaeoenvironmental conditions. In addition, the palaeoweathering of the studied samples appears to have substantially changed the carbon, oxygen, nitrogen and molybdenum stable isotope values. The nitrogen and molybdenum stable isotope ratios, in particular, appear to be most sensitive to the effects of weathering and therefore are good indicators

of (palaeo)weathering processes. The major cause of these changes is the decay of organic matter and pyrite. For the organic carbon stable isotopes ratios, the main factor that controlls this process appears to be the preferential degradation of labile organic matter. A combination of the total organic carbon (TOC), total sulphur (TS) content, Mo concentration and stable isotope compositions seems to be the most useful to identify (palaeo)weathering. Our results suggest that reductions in TS and Mo in tandem with diminished Mo stable isotope compositions in the absence of obvious changes to the TOC content provide the most compelling evidence of (palaeo)weathering.

Key words: weathering; redox conditions; inorganic proxies; REE; U/Th; Gd/Yb; stable isotopes

1. Introduction

Black shales that are deposited in oxygen-deficient environments are typically enriched in redox-sensitive elements, including sulphide-bound trace metals and elements that are involved in biological cycles (Georgiev et al., 2012). Experimentally defined inorganic palaeoenvironmental proxies (e.g., U/Th or Ni/Co ratios) are routinely used to reconstruct the redox conditions during the deposition of organic-rich sedimentary rocks (e.g., Rimmer, 2004; Riquier et al., 2005, 2006; Racka et al., 2010; Bond et al., 2013). Other commonly applied element-based indicators in geochemical studies can estimate the palaeoproductivity and detrital input (e.g., P/Al, Ba/Al, Ni/Al, Cu/Al, Racki et al., 2002, 2012; Tribovillard et al., 2006; Algeo and Ingall, 2007; Schoepfer et al., 2014), the influence of volcanic activity (e.g., Zr/Al, Fe/Ti, Racki et al., 2002; Pujol et al., 2006), and the degree of hydrothermal overprinting (e.g., Al/(Al+Fe+Mn), Fe/Ti, Racki et al., 2002; Brumsack, 2006). Carbon and nitrogen stable isotope values are also regularly utilized in palaeoenvironmental studies of both ancient and recent marine systems (e.g., Bauersachs et al., 2014; Obreht et al., 2014; Tulipani et al., 2014). However, these proxies are often measured in sedimentary rock samples collected from outcrops that have been exposed to atmospheric conditions for unknown periods. Weathering processes may thus have altered the elemental abundances and isotopic ratios, potentially creating misleading interpretations regarding the depositional redox conditions.

Previous studies have considered the loss of organic carbon induced by oxidation, the theoretical modelling of weathering pathways, and general variations in kerogen composition (Leythaeuser, 1973; Lo and Cardott, 1995; Bolton et al., 2006). Notably, pyrite appears to reacts more rapidly with O_2 than organic matter (OM) does, creating a deeper pyrite oxidation front than the OM weathering front (Petsch et al., 2000; Wildman et al., 2004; Bolton et al., 2006). Detailed studies of changes in the molecular composition of both extractable and unextractable OM (Clayton and King, 1987; Littke et al., 1989; Petsch et al., 2000; Marynowski et al., 2011a & b; Tamamura et al., 2015) have revealed the selective leaching of kerogen macromolecules and changes in soluble organic compounds' concentrations and distributions from the initial degradation of less stable biomarkers and

biomolecules. Numerous studies concluded that weathering processes can significantly influence the interpretation of biomarkers as palaeoenvironmental proxies and indicators of OM sources (Clayton and King, 1987; Petsch et al., 2000; Marynowski et al., 2011a & b).

The alteration of major and trace element compositions (including REEs) and stable isotope ratios caused by secondary hypergenic processes, including weathering and biodegradation, remains poorly understood. The mobility of rhenium and platinum group elements during weathering of organic-rich deposits has been addressed by Peucker-Ehrenbrink and Hannigan, (2000) and Jaffe et al. (2002), and Kolowith and Berner (2002) investigated the effects of weathering on phosphorus concentrations. Still, knowledge of the behaviour of many other elements is scarce. Thus, interpretations of palaeoenvironmental conditions based on conventional elemental proxies may be compromised by the effects of weathering (Georgiev et al., 2012).

Here, we investigate variations in the chemical composition of a Lower Carboniferous (Tournaisian) marine black shale horizon caused by palaeoweathering. We focus on progressive changes in major and trace elements, with special attention on the disturbance of key palaeoenvironmental proxies. In addition, we document the variations in $\delta^{13}C$, $\delta^{15}N$ and $\delta^{98}Mo$ from unweathered black shale to highly weathered rock. This study presents a unique opportunity to consider the effects of increasingly intense oxidative weathering along a single homogenous black shale bed (Fig. 1).

2. Samples and Methods

An interval of the open marine sedimentary sequence of the Holy Cross Mountains (Szulczewski, 1995) is exposed along the eastern wall of an active quarry in Kowala, Holy Cross Mountains, Poland (Fig. 1, cf. Marynowski et al., 2011a; 2012). A detailed geological description of this area and the Devonian-Carboniferous boundary section has been provided by Marynowski et al. (2000, 2010) and Berkowski (2002). Carboniferous and Devonian rocks dip steeply to the west and are overlain by a few meters of red Permian conglomerate, which is in turn overlain by Quaternary deposits. At the contact with Permian rocks the older rocks are visibly oxidized to a depth of a few meters, although individual layers are readily traced along the length of the exposure. A 10-cm-thick black shale horizon (KQ136; cf. Marynowski et al., 2011a) was selected for this study. The layer changes colour within the weathering zone as one approaches the contact with the Permian deposits first to green and then to red at the contact (Fig. 1). Nineteen samples were collected in September 2012 from a 3-4 cm thick interval at the bottom of the shale. Samples A to F represent black shale. Samples G to K were also black but with some rusty coatings, while samples L to T were green and change to red in the uppermost part (Fig. 1). Previous studies of Upper Devonian to Lower Carboniferous samples from the same quarry indicated that these rocks are thermally immature to early mature, with Rock-Eval T_{max} values between 421 and 425 °C and an average vitrinite reflectance value of 0.53% R_o (Marynowski and Filipiak, 2007; Marynowski et al., 2011a).

2.1. Total organic carbon (TOC) total sulphur (TS) total nitrogen (TN) and total hydrogen (H)

The total carbon (TC), total inorganic carbon (TIC) and total sulphur contents were determined by using an Eltra CS-500 IR-analyser with a TIC module. The TS and TC were determined by using an infrared cell detector for CO_2 and SO_2 gases, which evolved from the combustion of organic matter under an oxygen atmosphere with the simultaneous thermal decomposition of carbonates. The TIC content was determined by an infrared detector in which CO_2 that was derived from carbonates was reacted with 15% warm hydrochloric acid. The TOC was calculated as the difference between the TC and TIC. The instrument calibration utilized the Eltra standards.

Carbonate-free residues were analysed for the TOC, TN and H by using a Vario Micro Cube elemental analyser. The absolute precisions of the TOC, TN and H analyses were ±0.6%, ±0.18% and ±0.21%, respectively. The detection limits for the analytical procedures were ~ 40 ppm.

2.2. Organic matter pyrolysis (Rock Eval)

The Rock Eval 6 apparatus followed a "basic" protocol for OM pyrolysis. The protocol involved isothermal heating at 300 °C for 4 min at the beginning of pyrolysis followed by ramp heating to 650 °C at a rate of 25 °C /min, allowing determination of S1 and S2 parameters, which correspond to thermo-vaporized mobile hydrocarbons and those that produced by cracking, respectively (Behar et al., 2001). The S3 parameter, which representins oxygen-bearing OM compounds, was quantified by integrating the CO_2 signal at the temperature range that corresponded to the OM pyrolysis. In order to distinguish CO_2 generated by OM and from that produced by carbonate minerals at pyrolysis temperatures > 400 °C, powdered samples were re-analyzed after treatment with 10% HCl to remove carbonates (Behar et al., 2001; Derkowski and Marynowski, 2016).

2.3. Paleomagnetic studies

Six precisely oriented samples of the red, uniformly dipping, limestone layers approximately three meters below the palaeo-erosional surface and a meter below the investigated KQ136 black shale (Fig. 1c) were collected for palaeomagnetic analysis. This work involved the isothermal remnant magnetization (IRM), back-field demagnetization and thermal demagnetization of three-component IRM which was performed by using a 2G SQUID magnetometer with a MMPM10 pulse magnetizer. Hysteresis loops were then investigated by employing a MicroMag magnetometer. The structure of the natural remnant magnetization (NRM) was investigated by applying the thermal demagnetization technique and by using a SQUID magnetometer with a MM-1 furnace. After each thermal cleaning step, the magnetic susceptibility was monitored by applying a AGICO KLY3S kappabridge. Finally, the separation of paleomagnetic directions was carried out utilizing the software of Chadima and Hrouda (2006).

2.4. Trace metals analysis

Nineteen rock samples collected from the Carboniferous black shale horizon were analysed at AcmeLabs, Vancouver, Canada for major oxides and several minor elements (Ba, Ni, Sr, Zr, Y, Nb and Sc) by using ICP-emission spectrometry following a lithium borate fusion and dilute acid digestion of a 0.2 g sample pulp. Two separate ICP-MS analyses were performed to optimize the determination of a 31-element suite of trace elements (Ba, Be, Co, Cs, Ga, Hf, Nb, Rb, Sn, Sr, Ta, Th, U, V, W, Zr, Y, La, Ce, Pr, Nd, Sm, Eu, Gd, Tb, Dy, Ho, Er, Tm, Yb and Lu). The reliability of the analytical results was monitored by analysing international standard reference materials and duplicate analyses of a few samples. The precision and accuracy of the results were better than ±0.05% (mostly ±0.01%) for the major elements and generally better than ±1ppm for the trace elements.

2.5. Isotope studies

Powdered samples were reacted with 100% H_3PO_4 at 70°C to produce CO_2. Isotope measurements were conducted at the Isotope Dating and Environment Research Laboratory of the Institute of Geological Science, Polish Academy of Sciences, Warszawa (Poland) with a KIEL IV Device that was connected on-line to a Finnigan MAT Delta plus isotope ratio mass spectrometer. The results are reported relative to the PDB standard by using the NBS-19 reference sample. The reproducibility was better than ± 0.03 ‰ ($\delta^{13}C$) and ± 0.07 ‰ ($\delta^{18}O$).

The samples that were analysed for the carbon and nitrogen isotope composition of bulk organic matter ($\delta^{13}C_{org}$) were decarbonated in 10% HCl and rinsed with deionised water. The residues were weighed in tin capsules and introduced into a Thermo Flash EA 1112HT that was connected to a Thermo Delta V Advantage isotope ratio mass spectrometer at the IGS PAS (Warszawa). The standardization was based on the USGS 40, USGS 41, and IAEA 600 international standards. The isotope values are reported relative to the PDB ($\delta^{13}C_{ORG}$) standard and air N_2 reference standard ($\delta^{15}N$). The precision was better than ± 0.33‰ for $\delta^{13}C_{org}$ and ± 0.43‰ for $\delta^{15}N$.

Molybdenum isotope compositions were determined at the IGS PAS (Kraków, Poland) and at The Open University (UK). The analytical protocols for the chemical digestion and purification of Mo from shale powders are described in detail by Duan et al. (2010) and Liermann et al. (2011). The Mo isotope compositions were measured by using a combination of standard-sample bracketing and the Zr element spike method at IGS PAS (Anbar et al., 2001) and the double-spike method at the Open University (Pearce et al., 2009) to correct for instrumental mass fractionation. The $\delta^{98}Mo$ values are presented relative to an in-house Mo reference solution Alfa Aesar Specpure, ICP Mo solution standard at the IGS PAS and Fischer Chemicals, ICP Mo standard solution at The Open University according to the common δ calculation. The samples were analysed at least in triplicate. The instrument accuracy was verified by analysing the USGS Devonian Ohio black shale standard, SDO-1, which was processed in the same manner as the samples, and the NIST 3134 sample. The average $\delta^{98}Mo$ for SDO-1, based on three separate powder digestions, was + 1.12 ± 0.14‰ (external reproducibility; 2 S.D., IGS PAS), and that for NIST 3134 (OU) was + 0.37 ± 0.07‰ (2 S.D.). The isotopic differences among the samples that were measured at the laboratories were < 0.20‰.

3. Results and Interpretations

3.1. Age of palaeoweathering

The position of the weathering zone below the contact of the Tournaisian black shale and overlying Permian conglomerate suggests that the weathering occurred during the Permian.

Palaeomagnetic analysis can be used to estimate the age of palaeoweathering processes. As shown by numerous studies, oxidized fluids that infiltrate rocks from the surface significantly change the redox potential of pore fluids and thus result in the formation of new ferromagnetic minerals (e.g., Keller and Gehring, 1992 Franke et al. 2010). These newly growing ferromagnetic minerals become magnetized in the contemporaneous geomagnetic field. The orientation of this magnetization corresponds with the latitude of the continent at the time of weathering. The isolation of such a palaeomagnetic component enables the palaeoweathering episode to be dated by a comparison of the obtained virtual geomagnetic pole (VGP) with the reference apparent polar wander path (APWP) for the investigated continent.

The studied profile contains hematite as the dominant weathering product, as shown by both the red colour of the weathered rocks, quantitative XRD data, and petromagnetic analysis confirmed that the most common ferromagnetic mineral of the studied rocks was hematite (e.g. Fig. 2a & b). Most of the specimens contained some goethite and small amounts of low-coercivity magnetic minerals, most likely magnetite and maghemite. The analysed rocks were essentially resistant to AF demagnetization, which indicate that the remanence was mostly carried by high-coercivity hematite and goethite. During thermal cleaning, the lowest demagnetization temperatures removed the remanence that was carried by the goethite. At higher temperatures (up to 575°C), the magnetization only slightly decreases (Fig. 2c). However, this feature frequently displayed a somewhat more pronounced drop at 350-400°C, which was associated with the demagnetization of weak magnetic remanence with a roughly SSW declination and shallow inclination (before tectonic correction). At temperatures greater than 570°C, a strong, single hematite-bearing component was demagnetized, which indicates a maximum unblocking temperature (Tub) of 660°C. The component was calculated for 18 specimens giving the mean palaeomagnetic direction of 210/-38 (205/5 after tectonic correction) with k= 45 and α= 5.6. The corresponding VGP (before tectonic correction) matched the Permo-Triassic segment of the reference APWP (Fig. 2c).

Our palaeomagnetic observations corresponded well with previous results from the Holy Cross Mountains. A number of published studies have shown that the Devonian carbonates typically record one or two secondary components that are carried by magnetite and/or maghemite (B – normal polarity, syn-folding component; A - reversed polarity, post-folding component; see Zwing (2003) and Szaniawski (2008). In turn, carbonates that displayed a characteristic reddish shade were habitually remagnetized during the Permo/Triassic period as a result of infiltration by oxidizing fluids related to post-Variscan exhumation and karstification (post-folding Permo-Triassic component C carried by hematite – see e.g. Zwing 2003, Szaniawski at al. 2011). We assumed that the red carbonates that were investigated in these studies contained a weak residue of the A component (Tub 350-400°C, reversed polarity) that was almost completely overprinted by magnetization in hematite, the latter corresponding to remagnetization event C. The position of the VGP relative to the APWP

(Fig. 2c) in tandem with the results of previous studies (Szaniawski, 2008; Szaniawski at al., 2011) recorded the age of remagnetization and, therefore, palaeoweathering to be Late Permian.

The Permian age of weathering in the Kowala section was supported by a pattern of mineral transformations. The vermiculitization of chlorite, which was observed along the Tournaisian shale weathering transect, does not occur in chlorite in the Permian conglomerate, which confirms that the conglomerate did not participate in the weathering of the black shale (see Supporting Materials for details).

3.2. Geochemical proxy changes - enrichment and depletion patterns

3.2.1. Total organic carbon (TOC), total sulphur (TS), total nitrogen (TN) and Rock Eval data

The TOC and TS were measured along the black shale horizon by using two independent methods (Fig. 3; Table 1). Both methods showed a marked depletion in TOC and an absence of TS in the highly weathered zone, as previously observed by Marynowski et al. (2011a).

The TOC gradually decreased through the weathering zones from ~ 6% in the unweathered part to 0.3 - 0.05% in the highly weathered zone (Fig. 3). The oxidation of more than 99% of the organic carbon is consistent with very intense chemical weathering typical of warm tropical climates (Pope et al., 1995). The TS concentration decreased to zero in the highly weathered part of the shale (Fig. 3) as a result of the complete dissolution of sulphides (Wildman et al., 2004; Marynowski et al., 2011a).

The significant documented depletion in TOC and TS clearly would result in miscalculations of geochemical parameters that rely on the TOC, TS, and Fe contents, including the degree of pyritization (see Rimmer, 2004; Rimmer et al., 2004; Ross and Bustin, 2009). Assuming a constant Fe content (Fig. S2), the near complete depletion in TOC and TS significantly changed the calculated DOP depending on the actual position along the weathering transect (Fig. 4). The positions of the unweathered samples on the TOC-TS-Fe plot represent apparent dysoxic to slightly oxic conditions, whereas those of the partially weathered and weathered samples suggest a highly oxic sedimentary environment (Fig. 4).

The OM weathering trend presented by Rock Eval results was consistent with what has been presented elsewhere (Georgiev et al., 2012; see also Petsch et al., 2000). In all the samples, the S1 values that represented free hydrocarbons were ≤ 0.5 mgHC/g rock. The S2 values of the samples from the unweathered zone were 18-27 mg HC/g rock, while the S3 values were ~ 1.4 mg CO_2/g rock, which yielded Hydrogen Index (HI) values of ~ 300 mg HC/g TOC and Oxygen Index (OI) values of 20 mg CO_2/g TOC (Fig. 5). The T_{max} remained constant at 426 °C. These parameters correspond to an immature / early mature type II kerogen with possible type III admixtures (Fig. S4), which is consistent with the results of Marynowski and Filipiak (2007) and Marynowski et al. (2011a). The

consistently high HI and low OI values associated with the unweathered zone indicated that these deposits did not accumulate under oxygenated conditions (Landais et al., 1991; Rose et al., 1998; Faure et al., 1999; Petsch et al., 2000; Georgiev et al., 2012).

The boundary of the unweathered and partially weathered zones coincided with a reduction in S2 below 20 mg HC/g rock (Fig. 5). S2 displays an abrupt reduction in the middle of the transition zone. The decrease in S2 preceded the diminishing TOC as weathering progresses, so the HI in the middle of the transitional zone decreased to ~70 and then to 20 mgHC/g TOC, whereas the TOC remained relatively high (> 1 %). The OI increased before the significant decrease in the HI and TOC, reaching very high values of ~180 mg CO_2/g TOC (equivalent to ~ 0.1 O/C at.). Although the TOC in the weathered zone was too low to determine the Rock Eval parameters, the CO_2 that was produced by the pyrolysis of carbonate-free samples was above the background levels, which suggests that residual traces of OM were characterized by very high OI.

The nitrogen content correlated linearly with the TOC (R^2 = 0.99; Tables 1 and S1), extrapolating to 0.03% at 0% TOC. This observation implies very low ammonium content in the illite (compare Środoń and Paszkowski, 2011) and a very high N/C ratio of ca. 0.05, which are consistent with a high basic contribution from N-bearing functional groups in kerogen. Furthermore, these data indicated that the N/C ratio of the kerogen remained stable during weathering.

3.2.2. Distribution and partitioning of mobile and immobile elements

Trace elements and REEs are used as indicators of both sedimentary and diagenetic geochemical conditions, often without considering their distribution among the mineral components of the rock. Different rock matrix species can contribute to bulk rock elemental concentrations as outlined above, for the major mineral-forming elements (Section 3.2.3). The relationships of trace elements to the mineralogy are less predictable than those for major elements. Moreover, trace elements do not have strict crystallographic constraints as major elements do, which can occur in trace minerals that are undetectable or unquantifiable by routine bulk rock mineralogical analysis (McCarty et al., 2015). Trace elements can substitute for major elements in crystallographic positions or form trace minerals and, can be adsorbed onto clay mineral and organic particle surfaces or incorporated into organic structures (e.g., metalloporphyrins). The complete studied weathering profile, in which a major portion of the shale silicate matrix remained unaltered during weathering, provides an opportunity to differentiate mobile and immobile trace elements and distribute them quantitatively between mobile and immobile shale mineral compounds (for results and discussion on the mineral composition, see the Supporting Materials).

The mobile and immobile rock compounds were represented by different elements or parameters (cf. Fig. 3 and 5). Accordingly, Al was taken to represent the total (alumino-)silicate immobile portion, Fe was considered separately due to supergenic enrichment, the TIC represented the

calcite alteration pathway, and the total S was the most precise proxy for pyrite (especially S that was not incorporated onto OM structures; see Marynowski et al., 2011a). OM could be considered in terms of three different fractions: (1) the TOC which also correlated with N and represented N-bearing basic functional groups in kerogen;, (2) the total pyrolysable hydrocarbons (S2 parameter in Rock Eval); and (3) oxygen-rich functional groups (S3 parameter in Rock Eval). The partitioning of a given element whose concentration was measured in a sample (C_{meas}) was performed by using a multi-variable linear regression correlation:

$$Er = \sum [(S_{MOB} \times C_{MOB} + S_{IM} \times C_{IM}) - C_{meas}]^2 \quad (1)$$

where the contribution of an immobile component (S_{IM}) is represented by the Al concentration and the contribution from a mobile component (S_{MOB}) is represented by one of the following: TOC, TIC, Total-S, Fe, or the Rock Eval S3 parameter. The immobile and mobile compound coefficients C_{IM} and C_{MOB} was optimized by minimizing the global square error (Er) for each element. The lowest Er for an element that is tested with different mobile compounds thus represents the best model for that element and indicates the mobile shale compound that contributes the most to the mobile portion of the element (Table 2).

3.2.3. Uranium and thorium

The thorium to uranium ratio is frequently used as an indicator of palaeoenvironmental redox conditions during shale deposition (e.g. Jones and Manning, 1994; Tribovillard et al., 2006; Marynowski et al., 2012; Bond et al., 2013). Uranium is highly sensitive to variations in seawater redox conditions (e.g. Arthur and Sagemen, 1994; Wignall, 1994), whereas thorium is immobile, being insoluble in surface water and located in residual minerals during weathering (Jones and Manning, 1994). Under anoxic marine conditions, dissolved U^{6+} is reduced to U^{4+} and adsorbed or precipitated as uraninite or another insoluble uranium oxide. Under oxic conditions, U^{4+} is present as soluble hexavalent U^{6+} and uranyl carbonate ionic complexes that can migrate in aqueous solutions (Tribovillard et al., 2006; Pollack et al., 2009).

Thorium displayed a strong covariance with detrital clay minerals (see Supporting Materials). The Th concentration did not significantly change during weathering and reached ca. 11 ppm in the unweathered and partially weathered zones and ca. 12 ppm in the weathered zone of the black shale (Table S1). The uranium content displayed a weak positive correlation with the TOC but also correlated well with the oxygen functional groups of kerogen, as represented by the Rock Eval S3 peak (Table 2). The observed association with OM compounds explains why the U concentration significantly decreases from ca. 10 ppm in the unweathered black shale to ca. 4 ppm in the weathered

samples (Table S1). Consequently, the U/Th ratio values decreased from ca. 1 in the unweathered samples (indicating dysoxic sedimentary conditions), to values that ranged from 0.31 to 0.50 (Table 1; Fig. 3), which are typically interpreted to reflect oxic water column (see Arthur and Sagemen, 1994; Racka et al., 2010). A similar decrease in the calculated U_{auth}, which mimic the dysoxic-oxic transition, was observed through the weathering zones (Table 1).

The oxidative dissolution of uranium has been discussed in earlier studies. For example, Tribovillard et al. (2006) noted that the post-depositional re-oxygenation and early diagenetic remobilization of U, caused U depletion in underlying sediments from the influence of turbidites. Dalai et al. (2002), determined that weathered silicates may be an important source of U in Himalayan rivers based on the correlation of U with ∑Cations, and Tuttle et al. (2009) observed a decrease in the U concentration from the unweathered towards the exposed and weathered New Albany Shale, linking this feature to OM oxidation. Moreover, Pollack et al. (2009) demonstrated that post-depositional processes could alter the Th/U ratio due to the selective removal of uranium by oxygenated fluids. Similarly, our study documents the degree to which U depletion caused by palaeoweathering modified the Th/U and palaeoredox interpretations based on the use of Th/U ratios. Whereas the fully weathered zone could be visually identified and, therefore, avoided in palaeoenvironment proxy studies, the black shale in the partially weathered zone retained its dark appearance, precluding the recognition of its weathering history. The U/Th (and Th/U) redox proxy should thus be used with caution in cases where samples were exposed to past or present weathering.

3.2.4. Nickel, cobalt and molybdenum

Nickel is commonly used as a redox-sensitive element (Tribovillard et al., 2006; Brumsack, 2006). Under oxic marine conditions, Ni is present as soluble cations (Ni^{2+} or $NiCl^{+}$) and Ni carbonate or can be adsorbed onto complex humified organic acids (Tribovillard et al., 2006). Under reducing conditions, Ni is incorporated into pyrite (as NiS) or tetrapyrolle complexes (geoporphyrins) and trapped in sediments (Baker and Louda, 1986; Tribovillard et al., 2006). Two approaches that are based on the Ni content are widely used in environmental proxy parameters, including the V/(V+Ni) ratio, which was defined by Hatch and Leventhal (1992), and the Ni/Co ratio, which was described by Jones and Manning (1994).

In both cases, the element ratios significantly change as a consequence of weathering (Figs. 3 & S5; Table 1). These changes were caused by coupled Ni and TOC depletion in the upper part of the transitional zone and the highly weathered zone (Table S1), while V that was distributed between the silicate minerals and oxygen-bearing functional groups in kerogen increased in the partially weathered zone (Table 2, Figs. 3 & S5). Therefore, the V/(V+Ni) ratio increased in response to increased weathering. Notably, the V/(V+Ni) values of the unweathered samples from the studied black shale

horizon are typical of dysoxic conditions, whereas the V/(V+Ni) ratios of the samples from the partially weathered and highly weathered zones are characteristic of anoxic conditions (Fig. 3).

Although Co and Ni were distributed among similar rock components, the silicate matrix's contribution to the bulk Co was much less than that to the bulk Ni content, which implies a higher contribution from element-mobile OM components (C_{MOB} / C_{IM} were 1.75 and 16.1, respectively; Table 2). This observation explains the significant increase in the Ni/Co ratio at the weathering front of the studied black shale (Table S1; Fig. 3). Brumsack (2006), after Huerta-Diaz and Morse (1992), suggested that pyrite is moderately important as a carrier phase of Co and Ni. This view is consistent with our results, even if in some cases pyrite was the dominant Ni-bearing phase in the black shales (Yu et al., 2014; Perkins and Mason, 2015). A similar decrease in Ni concentration in the weathered New Albany Shale was noted by Tuttle et al. (2009), but Ni was principally located in pyrite in this case. Grosjean et al. (2004) documented a significant decrease in nickel and vanadyl porphyrin concentrations because of weathering, which would be an important process of Ni removal in the weathering and transitional zones of the studied black shale horizon (Table S1). However, the Ni/Co ratio values increased from the unweathered toward the weathered zone, which suggests that the rate of loss of Co was higher than the rate of loss of Ni for the studied black shale (Fig. 3).

Molybdenum is another element whose behaviour is strongly dictated by the redox conditions (Morford and Emerson, 1999; Lyons et al., 2003; Brumsack, 2006). Its concentrations are especially high in persistently anoxic and sulphidic environments because MoO_4^{2-} reacts with HS^- to create thiomolebdates, which are often bound to iron sulphides (Helz et al., 1996; Morford and Emerson, 1999; Tribovillard et al., 2006).

Our results demonstrated a very rapid depletion in Mo across the weathering profile of the black shale horizon (Fig. 3; Tables 1, 2 & S1). A strong correlation with the TS ($R^2 = 0.85$), low contributions from immobile mineral phases (Table 2), and a modest correlation with the TOC ($R^2 = 0.69$; see also Table 2) suggested that pyrite and less likely MoS were the main hosts of Mo in the Lower Carboniferous black shale (compare with Huerta-Diaz and Morse 1992; Tuttle et al., 2009). The rapid weathering of pyrite (Wildman et al., 2004) and consequent removal of Mo from black shale has important implications in the reconstruction of redox conditions based on the Mo concentrations of samplesthat are recovered from outcrops where the effects of partial weathering are not evident. However, Perkins and Mason (2015) observed no correlation between the Mo concentration and weathering, suggesting that Mo distribution is connected with multiple phases, including Mn-oxides or OM. Although the incorporation of Mo into diffuse Mo-sulphides was not ruled out by Perkins and Mason (2015), such a scenario seems less likely for the observations in our study. Interestingly, the Mo concentration minimally increased deeper into the weathered zone, where additional supergene Fe was also identified (compare Figs. 3 and S3).

Mo and U undergo differing degrees of enrichment depending on the bottom-water conditions, so the relative levels of authigenic enrichment in Mo and U in unaltered shale samples is a useful

measure of the bottom-water palaeoredox environment (Tribovillard et al., 2012). Trace element enrichment factors are calculated by comparing the measured values with the average crustal abundances, with the values normalized to the Al abundance to consider the effects of biogenic components. The Mo and U enrichment factors of the samples in this study, which were calculated by using equation (1) from Tribovillard et al. (2012) and normalized to the average upper crustal Mo, U and Al values of Rudnick and Gao (2003), covered a wide range. The samples from the unweathered part of the profile yielded results that were consistent with deposition under suboxic conditions in an unrestricted marine setting (Fig. 7A; see Algeo and Tribovillard, 2009; Tribovillard et al., 2012). Whilst the U abundances were >1 in all the samples, reaching a maximum enrichment > 4 in the unweathered samples, the Mo enrichment factors were substantially lower. Only 6 of the unweathered samples showed Mo enrichment greater than 1, and none greater than 3 (Fig. 6A). All the partially or intensely weathered samples showed substantial Mo depletion compared to the average crustal values (Fig. 6B).

3.2.5. Vanadium and chromium

The vanadium to chromium elemental ratio has been frequently used as an indicator of bottom water redox proxy (e.g., Jones and Manning, 1994; Racki et al., 2002; Rimmer, 2004; Rimmer et al., 2004; Pujol et al., 2006). Anoxic marine conditions favour the concentration of vanadium in organic matter by the incorporation of V^{4+} into porphyrins whereas chromium is often concentrated in the detrital sediment fraction (see Jones and Manning, 1994 and references therein). However, some amount of V may be transported to basins with detrital silicate (clay) minerals (Wignall, 1994; Tuttle et al., 2009). Our results showed small changes in the V/Cr ratio with increasing weathering (Fig. S5). The magnitude of the ratio corresponded to generally oxic conditions (Table 1). Vanadium only increased in the enrichment zone (see below), where the V/Cr ratio values were characteristic of oxic conditions (cf. Jones and Manning, see also Rimmer, 2004). The chromium distribution in the black shale was controlled by the immobile matrix contribution, with minor contributions from pyrite (Table 2).

3.2.6. Nb and Ti vs. Cr

The Cr/Ti and Cr/Nb ratios were considered by Środoń et al. (2014) as the most stable indicators of the provenance (to discriminate between mafic and acidic rocks) and were successfully used to correlate continental sediments in the Silesan Keuper. Our study confirmed the invariance of the Cr/Ti and Cr/Nb ratios during weathering (Table S1).

3.2.7. Rare earth elements (REE)

REE concentrations, particularly Ce (e.g., Frimmel, 2009), have been cited as sensitive indicators of palaeoredox conditions (Liu et al., 1988; German and Elderfield, 1990; however see doubts raised by Lev and Filer, 2004).

REEs are generally assumed to be conservative during weathering processes and are transported to the ocean with the fine-grained suspended sediment fraction (Pollack et al., 2009). Nevertheless, McArthur and Walsh (1984) suggested that oxidative weathering may 1) alter the abundances of REEs and 2) selectively remove light REEs (LREEs) at a greater rate than that at which heavy REEs (HREEs) are mobilized. Hannigan and Sholkovitz (2001) experimentally showed that the weathering of shale and consequent dissolution of phosphate minerals cause depletion inf REEs, especially middle REEs (MREEs). Recently, Ma et al. (2011) postulated that weathering-related processes preferentially remove MREEs.

The total REEs of the samples that were analysed in our study decreased toward the weathered zone (Table S1 & S2; Fig. S6), and the REE depletion pattern was similar to what was documented by Ma et al. (2011), who observed the preferential loss of MREEs. Indeed, Sm, Eu and Gd displayed losses of 30%, 25% and 26%, respectively, between the unweathered and weathered zones, which are 10% to 30% greater than the measured differences for LREEs and HREEs (Fig. 7). Furthermore, some differences were noted in the REE ratios (e.g., Ce/Ce*, Eu/Eu*, La/Yb, Ce/Yb, La/Sm or Gd/Yb). The highest discrepancies were noted for the Gd/Yb ratio, with the difference between the unweathered and weathered samples reaching 35%.

Our data suggested that the REE concentrations from La to Dy were controlled by both immobile compounds and OM, with very similar C_{MOB} / C_{IM} ratios of 0.25-0.41 (Table 2). These results related the marked change in REE concentrations from the unweathered to completely weathered shale (Fig. 7), which was related to diminished TOC (Fig. 3). The Lu concentration almost exclusively depended on immobile compounds, with little contribution from OM. The Tm and Yb concentrations were independent of the TOC content and seemed to be strongly controlled by carbonate minerals (Table 2). However, their abundance patterns did not change despite major carbonate dissolution. The Ho and Er concentrations did not show any clear correlation with any particular immobile components.

3.2.8. TOC/P ratio

Algeo and Ingall (2007) advocated the use of the C_{org}/P ratio as a robust proxy for productivity and bottom-water redox conditions. Increased levels of organic matter burial under anoxic bottom results in the simultaneous remobilization and escape of phosphorous from sediment into the water column (Tribovillard et al., 2006; Algeo and Ingall, 2007). However, oxic conditions favour the sequestration of organic P in sediment by incorporation into Fe-oxyhydroxides or authigenic

carbonate-fluoroapatite phases (Slomp et al., 1996; Tribovillard et al., 2006; Algeo and Ingall, 2007) and the degradation of organic matter. Studies of modern marine environments suggested that the C_{org}/P ratio of sediment that is deposited under permanently anoxic conditions > 150 whereas sediment that accumulated under oxic bottom-water conditions is characterized by C_{org}/P < 30. Intermediate values indicate dysoxic conditions (cf. Algeo and Ingall, 2007; Mort et al., 2010).

Our results showed very rapid depletion in C_{org} and a consequent decrease in C_{org}/P in the weathering profile (Table 1). The samples from the unweathered zone to the middle of the partially weathered zone displayed C_{org}/P values > 150, which are typical of anoxic conditions and/or high-productivity regimes. The samples from that part of the partially weathered zone that was adjacent to the weathered zone were defined by intermediate C_{org}/P values, which indicate a dysoxic but high-productivity regime. The samples from the interior of the weathered zone displayed Corg/P ratio values < 10 (Table 1), which are typical of oxygenated, low-productivity regimes. These results are in agreement with the observations of Kolowith and Berner (2002) who maintained that the dominant P compounds in shales are P esters, which are highly resistant to chemical weathering. The results of Kolowith and Berner (2002) can explanin the stability of P from unweathered into weathered black shale even as C_{org}/P diminishes because of a loss of organic C. However, the very low C_{org}/P values deeper in the weathering zone (< 7; Table 1) suggest the role of an additional mechanism responsible for the P accumulation, for example, the binding of P by iron oxides (Slomp et al., 1996).

Barium and silica are also sometimes used as palaeoproductivity proxies (e.g. Schmitz et al., 1997; Brumsack, 2006; Pujol et al., 2006; Śliwiński et al., 2011; Racki et al., 2012). No major changes in their contents were observed through the weathering section that was studied here.

3.3. Enrichment zone

Some elements appeared to have preferentially accumulated in that part of the transitional zone that was adjacent to the weathered zone (Fig. 8). All these elements (Cu, Pb, U and V) displayed a very strong correlation with the Rock Eval S3 parameter and, a strong correlation with TOC if we eliminate the samples 136J and 136K.

The Rock Eval S3 parameter increases during weathering-related oxidation (Petsch et al., 2000; Derkowski and Marynowski, 2016). We suggest that the ketone and carboxyl groups that form as a consequence of kerogen oxidation by migrating fluids can adsorb some cationic species (Derkowski and Marynowski, 2016) because these functional groups produce negative charges on the OM's surface. This mechanism explains both the correlation of Cu, Pb, U, and V with the Rock Eval S3 parameter and, the enrichment in these elements in the upper part of the partially weathered zone (Fig. 8).

Cu, Pb, U and V formed a group that was partially adsorbed onto the surface of OM, some of which originated from nascent kerogen with another fraction that originated from the immobile shale

matrix. The order of mobility, Cu > Pb > U > V, is expressed in the C_{MOB} / C_{IM} ratios (Table 2). Interestingly, a small portion of the bulk Ba also appeared to have been adsorbed by OM and concentrated in the enrichment zone (Table 2). All these heavy elements are preferably adsorbed when mobilized under oxidizing solutions. We believe that these elements were mobilized by meteoric water from overlying horizons and preferentially bound by carboxyl groups in the partially weathered zone, where the Oxygen Index values were highest (Fig. 5). The TOC content in the highly weathered zone rapidly decreased, which prevented the binding of heavy elements to kerogen. This enrichment zone could mark the position where migrating oxidation fronts temporarily halted and thereby concentrated some elements.

3.4. Variations in stable isotopes through the weathering zone

3.4.1. Organic carbon isotopes

Variations in the $\delta^{13}C$ of organic matter ($\delta^{13}C_{org}$) are usually interpreted in terms of changes in the burial rate; varying contributions from terrigenous and marine organic carbon to basins, and changes in productivity and atmospheric pCO_2 levels (e.g., Popp et al., 1997; Kump and Arthur, 1999; Berner, 2002; Averbuch et al., 2005; Chen et al., 2005).

The $\delta^{13}C_{org}$ values of nine samples from the unweathered section in the partially weathered zone defined a narrow range from -27.6‰ to -27.9‰ (Fig. 9). However, six samples from the partially weathered zone into the weathered zone displayed a 3‰ increase that peaked within the weathered zone, beyond which $\delta^{13}C_{org}$ decreased to the isotopic composition of the unweathered shale (ca. -27.7‰; Fig. 9).

Clayton and Swetland (1978) observed a similar, ~3‰ shift in the near-surface weathered zone of the Permian Phosphoria Formation (NE Utah). These authors suggested that the destruction of aromatic structures during weathering is accompanied by the preferential loss of compounds that are enriched in the ^{12}C isotope. The preferential removal of isotopically 'light' carbon due to oxidation which leads to enrichment in ^{13}C in the residual bulk organic matter, was also reported by Sackett and Thompson (1963); similar processes could be responsible for the observed isotopic shifts in our study. A sharp drop in $\delta^{13}C_{org}$ in the weathered zone close to the partially weathered zone (Fig. 9) correlated with an increase in the Fe/Al ratio, perhaps indicating the transport of fine hematite and goethite particles down from the weathering front. One possible explanation for the $\delta^{13}C_{org}$ values within the same zone is the downward migration of dissolved organic matter or fine soil OM particles that are enriched in ^{12}C (see below).

3.4.2. Nitrogen isotopes

Nitrogen isotopic ratios have been used to trace changes in the degree of nitrate utilization, denitrification, and N_2-fixation (e.g., Macko et al., 1993; Freudenthal et al., 2001; Lehmann et al., 2002). Additionally, changes in bulk sedimentary $\delta^{15}N$ values can be linked with palaeoclimate fluctuations (Algeo et al., 2014; Rooney et al., 2015).

The samples from the unweathered zone were characterized by relatively low $\delta^{15}N$ values, ranging from 0.5‰ to 1.9‰ (Fig. 9). The samples from the partially weathered zone displayed generally higher but variable $\delta^{15}N$ values ranging from 1.3‰ to 4.6‰ (Fig. 9). The total nitrogen contents of the samples from the weathered zone were less than 0.1%, insufficient for $\delta^{15}N$ analysis.

Potential mechanisms responsible for ^{15}N isotopic enrichment include the preferential loss of ^{14}N due to organic matter decomposition, kinetic isotopic fractionation during protein hydrolysis and deamination and bacterial growth (Lehmann et al., 2002; Möbius, 2013). In this study, the degradation of less resistant organic compounds that were enriched in ^{14}N was likely the primary cause of documented changes in $\delta^{15}N$ across the weathering profile.

In some phytoplankton and bacterial cultures, the total protein within a cell is enriched in ^{15}N (~3‰) relative to the bulk nitrogen content (Macko et al., 1987). The aerobic bacterial decomposition of the organic matter liberates isotopically light ammonium into sediment porewaters (deamination; Macko et al., 1987) including ^{15}N enrichment of the residual organic matter as high as 6‰ (Altabet, 1988; Saino, 1992; Altabet and Francois, 1994, Lehmann et al., 2002). The bacterial biomass, that is produced during the degradation process may also operate as a substrate for further degradation. Under anoxic conditions, N-isotopic alteration during organic matter degradation is minimal (Sachs and Repeta, 1999), while the intensive microbial recycling and resynthesis of organic matter is frequently observed under oxic environments (Gong and Hollander, 1997). An increase in $\delta^{15}N$ due to organic matter oxidation was observed in suspended particulate matter (for example, the laboratory experiments of Lehmann et al., 2002) and, in burn sapropels (Lehman et al., 2002; Möbius et al., 2013; Algeo et al., 2014). Our observations are in line with these earlier findings, but the specific mechanism remains unclear.

3.4.3. Carbonate carbon and oxygen isotopes

Variations in the isotopic composition of marine dissolved inorganic carbon have been interpreted in terms of the effects on redox balances in the carbon cycle and the changes in palaeoproductivity and the burial of carbon (i.e., Popp et al., 1989; Kump and Arthur, 1999). The oxygen isotope ratio is a powerful proxy to reconstruct oceanic palaeotemperatures and the salinity of ancient oceans (e.g., Joachimski et al., 2004).

The $\delta^{13}C_{carb}$ values of the shales investigated here varied from -2.6‰ to -0.7‰ (Fig. 9). The samples from the unweathered zone and weathered zone that was adjacent to the partially weathered zone displayed $\delta^{13}C_{carb}$ values of -1.4‰ (Fig. 9). The highest $\delta^{13}C_{carb}$ values were documented from a sample along the boundary of the partially weathered and weathered zones (Fig. 9). The lowest $\delta^{13}C_{carb}$

values (average of -2.4‰) coincided with the samples from the area of the partially weathered zone that was adjacent to the unweathered zone and the samples collected from deeper within the weathered zone (Fig. 9). This observed trend of weathering-induced alteration did not follow that of $\delta^{13}C_{org}$, which suggests that the labile OM fraction did not control the $\delta^{13}C_{carb}$ variability.

□□¯ $\delta^{18}O$ values ranged from -5.1‰ to -4.0‰ and reached their maximum values in the unweathered and partially weathered zones (Fig. 9; Table 3). A cross-plot of the oxygen and carbon stable isotope values from the unweathered samples, in which the $\delta^{13}C$ rangeed from -1.1‰ to -1.5‰ and the $\delta^{18}O$ ranged from -4.2‰ to -4.7‰ showed limited variation, which suggests a low degree of diagenetic alteration of the calcite material (Table 3).

Carbonate minerals are more reactive and soluble than silicate minerals and often weather preferentially (Williams et al., 2007). For instance, carbonates are almost depleted in surface horizons of soil profiles where rainfall is abundant (Brantley et al., 2013). A small but distinct positive shift in $\delta^{13}C$ and less pronounced $\delta^{18}O$ increase at the boundary between the partially weathered and the completely weathered zones probably recorded calcite precipitation with an uptake of heavy $\delta^{13}C$ and $\delta^{18}O$, similar to what was described by Rachidi et al. (2009).

The highly weathered part of the horizon was depleted in carbonate because of the infiltration of freshwater that was enriched in CO_2 and/or organic acids (see Littke et al., 1991; Brantley et al., 2013). Isotopically light meteoric water and CO_2 present in the soil zone commonly cause a marked decrease of ^{13}C and ^{18}O in carbonates that underlay such soils (Allan and Matthews, 1982; Immenhauser et al., 2002).

The downward migration of O_2 -bearing fluids resulted in the oxidation of pyrite and the release of H_2SO_4, which increased the porosity and thus enabled the further infiltration of meteoritic fluids (Brantley et al. 2013). The first mineral that H_2SO_4 was likely to dissolve is carbonate. The weathered part of the horizon with a larger open pore volume, might have allowed the infiltration of larger volumes of isotopically light fluids, facilitating the precipitation of isotopically light carbonates in the weathering zone (Brantley et al., 2013).

3.4.4. Molybdenum isotope data

The molybdenum stable isotope system provides a valuable tool to assess ocean palaeoredox conditions (Barling et al., 2001; Siebert et al., 2003; Pearce et al., 2008). The mobilization of Mo from terrigenous material during weathering, erosion, and sediment transport under Mo-bearing fluids is a major source of dissolved Mo in seawater (Siebert et al., 2003; Reitz et al., 2007). Under oxidizing marine conditions, light Mo is selectively removed from the water column by adsorption onto ferromanganese phases and other authigenic minerals. Thus, preferential fractionation enriches the seawater in heavy isotopes ($\delta^{98}Mo$ ~2.3‰, Siebert et al., 2003; Arnold et al., 2004, Pearce et al., 2008). In contrast, Mo fractionation is not observed in water masses in which the sulphide

concentrations exceed 100 μM due to the rapid formation of thiomolybdates (e.g., Erickson and Helz, 2000; Arnold et al., 2004; Nägler et al., 2005; Poulson et al., 2006).

The studied horizon appears to have accumulated under generally dysoxic conditions (Marynowski et al., 2011a; see above). Mo fractionation in dysoxic water masses yields $\delta^{98}Mo_{(Seawater–Suboxic)}$ values from approximately 0.8 to 2.2‰ (Goldberg et al., 2009) and typical values of ca. 1‰ (Siebert et al., 2006). Our δ^{98}Mo data were dispersed within this range (Fig. 9; Table 3). The Mo isotope ratios of the samples from the weathered and partially weathered zones corresponded to ratios that are characteristic of continental rocks (δ^{98}Mo = ~0.0‰; Barling et al., 2001) and oxic sediments that were deposited under oxic conditions. Moreover, Mo abundances of these samples are very low (Fig. 3). As discussed in section 3.2.4, the calculated Mo enrichment factors relative to the average upper continental crust indicated that Mo was highly depleted in all the samples from the highly weathered zone and some samples from the partially weathered zone. The Mo isotope compositions of these samples were dominated by the residual Mo in the detrital siliciclastic component and thus could not provide information on the palaeoredox conditions in seawater. In contrast, the δ^{98}Mo values of the samples from the unweathered zone increased to ~1.15‰, which were characteristic of the suboxic (to anoxic) conditions of continental margin settings (Dickson et al., 2014).

4. Conclusions

Palaeomagnetic observations showed that the Devonian/Carboniferous sedimentary rocks of the Holy Cross Mountains, Poland, were weathered during the Permo/Triassic period (most likely Late Permian) as a result of the downward migration of oxidizing fluids related to post-Variscan exhumation and karstification processes. The weathering processes involved the dissolution of calcite and pyrite, precipitation of hematite and goethite, and vermiculitization of chlorite, which were specific to the Tournaisian black shale while the overlaying Permian conglomerate remained unweathered.

Values of widely used palaeoenvironmental geochemical proxies, including U/Th, Ni/Co, Mo, and V/Cr, displayed varying degrees of weathering-related alteration. Even apparently (visually) pristine black shale can manifested by modified concentrations of proxy elements. Moreover, the concentrations of Cu, Pb, U and V in the transitional area between the weathered and unweathered shale probably reflects the sorption of elements that were released from oxidized rock onto oxidized organic matter. Elements that are bound to iron sulphides (e.g., Mo) are especially prone to weathering-related mobilization, even in weakly weathered black shale. Thus, their altered measured concentrations and isotopic compositions did not reflect the initial sedimentary conditions.

Palaeoweathering appeared to significantly change the carbon, oxygen, nitrogen and molybdenum stable isotope compositions, principally as a consequence of changes in organic matter and pyrite degradation. The nitrogen and molybdenum stable isotope compositions were most sensitive to the effects of weathering. Not only outcrop samples are susceptible to the effects of recent weathering, and the borehole samples had to be treated with caution because they could have been affected by palaeoweathering events.

The visual inspection of rock and TOC determinations is not sufficient to recognize deposits that have been affected by weathering. A combination of the TOC and TS contents alongside the Mo concentration and molybdenum stable isotope composition can be useful to identify the effects of weathering. If the TS content, Mo concentration, and Mo stable isotopes significantly decrease without any changes in the TOC content, the section was likely affected by weathering.

Acknowledgments LM and AP acknowledge financial support from the Polish National Science Centre (grants 2011/01/B/ST10/01106 and UMO-2011/03/B/ST10/04602).

References

Algeo, T.J., Ingall, E.D., 2007. Sedimentary C_{org}:P ratios, paleocean ventilation, and Phanerozoic atmospheric pO_2. Palaeogeography, Palaeoclimatology, Palaeoecology 256, 130–155.

Algeo, T.J., Tribovillard, N., 2009. Environmental analysis of paleoceanographic systems based on molybdenum–uranium covariation. Chemical Geology 268, 211–225.

Algeo, T.J., Meyers, P.A., Robinson, R.S., Rowe, H., Jiang, G.Q., 2014. Icehouse–greenhouse variations in marine denitrification. Biogeosciences 11, 1273–1295.

Allan, J.R., Matthews, R.K., 1982. Isotope signatures associated with early meteoric diagenesis. Sedimentology 29, 797–817.

Altabet, M.A., 1988. Variations in nitrogen isotopic composition between sinking and suspended particles: implications for nitrogen cycling and particle transformation in the open ocean. Deep Sea Res. Part A 35, 535–554.

Altabet, M.A., Francois, R., 1994. Sedimentary nitrogen isotopic ratio as a recorder for surface nitrate utilization. Global Biogeochemical Cycles 8, 103–116.

Arnold, G.L., Anbar, A.D., Barling, J., Lyons, T.W., 2004. Molybdenum isotope evidence for widespread anoxia in mid-Proterozoic oceans. Science 304, 87–90.

Arthur, M.A., Sagemen, B.B., 1994. Marine black shales: Depositional mechanisms and environments of ancient deposits. Annual Review of Earth and Planetary Sciences 22, 499–551.

Averbuch, O., Tribovillard, N., Devleeschouwer, X., Riquier, L., Mistiaen, B., Van Vliet-Lanoe, B., 2005. Mountain building-enhanced continental weathering and organic carbon burial as major causes for climatic cooling at the Frasnian–Famennian boundary (c. 376 Ma)? Terra Nova 17, 25–34.

Baker, E.W., Louda, J.W., 1986. Porphyrins in the geological record. In: Biological Markers in the Sedimentary Record (ed. Johns R.B.), 125–225. Amsterdam: Elsevier.

Barling, J., Arnold, G.L., Anbar, A.D., 2001. Natural mass-dependent variations in the isotopic composition of molybdenum. Earth and Planetary Science Letters 193, 447–457.

Bauersachs, T., Schouten, S., Schwark, L., 2014. Characterization of the sedimentary organic matter preserved in Messel oil shale by bulk geochemistry and stable isotopes. Palaeogeography, Palaeoclimatology, Palaeoecology 410, 390–400.

Behar, F., Beaumont, V., De B. Penteado, H.L., 2001. Rock-Eval 6 Technology: Performances and Developments. Oil & Gas Science and Technology – Revue d'IFP Energies nouvelles 56, 111–134.

Berkowski, B., 2002. Famennian Rugosa and Heterocorallia from Southern Poland. Palaeontologia Polonica 61, 3–88.

Berner, R.A., 2002. Examination of hypotheses for the Permo–Triassic boundary extinction by carbon cycle modeling. Proceedings of the National Academy of Sciences of the United States of America 99, 4172–4177.

Bolton, E.W., Berner, R.A., Petsch, S.T., 2006. The weathering of sedimentary organic matter as a control on atmospheric O2: II. Theoretical modeling. American Journal of Science 306, 575–615.

Bond, D.P.G., Zatoń, M., Wignall, P.G., Marynowski, L., 2013. Evidence for shallow-water anoxic "Kellwasser Events" in the Frasnian-Famennian reefs of Alberta, Canada. Lethaia 46, 355–368.

Brantley, S.L., Holleran, M.E., Jin, L., Bazilevskaya, E., 2013. Probing deep weathering in the Shale Hills Critical Zone Observatory, Pennsylvania (USA): the hypothesis of nested chemical reaction fronts in the subsurface. Earth Surface Processes and Landforms 38, 1280–1298.

Brumsack, H.-J., 2006. The trace metal content of recent organic carbon-rich sediments: implications for Cretaceous black shale formation. Palaeogeography, Palaeoclimatology, Palaeoecology 232, 344–361.

Chadima, M., Hrouda, F., 2006. Remasoft 3.0 a userfriendly paleomagnetic data browserand analyzer. Travaux Geophysique 27, 20–21.

Chen, D., Qing, H., Li, R., 2005. The Late Devonian Frasnian–Famennian (F/F) biotic crisis: insights from δ^{13}Ccarb, δ^{13}Corg and $^{87}Sr/^{86}Sr$ isotopic systems. Earth and Planetary Science Letters 235, 151–166.

Clayton, J.L., Swetland, P.J., 1978. Subaerial weathering of sedimentary organic matter. Geochimica et Cosmochimica Acta 42, 305–312.

Clayton, J.L., King, J.D., 1987. Effects of weathering on biological marker and aromatic hydrocarbon composition of organic matter in Phosphoria shale outcrop. Geochimica et Cosmochimica Acta 51, 2153–2157.

Dalai, T.K., Singh, S.K., Trivedi, J.R., Krishnaswami, S., 2002. Dissolved rhenium in the Yamuna River System and the Ganga in the Himalaya: Role of black shale weathering on the budgets of Re, Os, and U in rivers and CO_2 in the atmosphere. Geochimica et Cosmochimica Acta 66, 29–43.

Derkowski, A., Marynowski, L., 2016. Reactivation of cation exchange properties in black shales. International Journal of Coal Geology 158, 65–77.

Dickson, A.J., Cohen, A.S., Coe, A.L., 2014. Continental margin molybdenum isotope signatures from the early Eocene. Earth and Planetary Science Letters 404, 389–395.

Duan, Y., Anbar, A.D., Arnold, G.L., Lyons, T.W., Gordon, G.W., Kendall, B., 2010. Molybdenum isotope evidence for mild environmental oxygenation before the Great Oxidation Event. Geochimica et Cosmochimica Acta 74, 6655–6668.

Erickson, B.E., Helz, G.R., 2000. Molybdenum (VI) speciation in sulfidic waters: stability and lability of thiomolybdates. Geochim. Cosmochim. Acta 64, 1149–1158.

Faure, P., Landais, P., Griffault, L., 1999. Behavior of organic matter from Callovian shales during low-temperature air oxidation. Fuel 78, 1515–1525.

Franke, C., Gomez-Gras, D. et al. 2010. Paleomagnetic age constrains and magnetomineralogic implications for the Triassic paleosurface in Europe. Geophysical Research Abstracts, 12, EUG2010-7858.

Freudenthal, T., Wagner, T., Wenzhöfer, F., Zabel, M., Wefer, G., 2001. Early diagenesis of organic matter from sediments of the eastern subtropical Atlantic: evidence from stable nitrogen and carbon isotopes. Geochimica et Cosmochimica Acta 65, 1795–1808.

Frimmel, H.E., 2009. Trace element distribution in Neoproterozoic carbonates as palaeoenvironmental indicator. Chemical Geology 258, 338–353.

Georgiev, S., Stein, H.J., Hannah, J.L., Weiss, H.M., Bingen, B., Xu, G., Rein, E., Hatlø, V., Løseth, H., Nali, M., Piasecki, S., 2012. Chemical signals for oxidative weathering predict Re–Os isochroneity in black shales, East Greenland. Chemical Geology 324–325, 108–121.

German, C.R., Elderfield, H., 1990. Application of the Ce anomaly as a paleoredox indicator: the ground rules. Paleoceanography 5, 823–833.

Goldberg, T., Archer, C., Vance, D., Poulton, S.W., 2009. Mo isotope fractionation during adsorption to Fe (oxyhydr)oxides. Geochimica et Cosmochimica Acta 73, 6502–6516.

Gong, C., Hollander, D.J., 1997. Differential contribution of bacteria to sedimentary organic matter in oxic and anoxic environments, Santa Monica Basin, California. Organic Geochemistry 26, 545–563.

Grosjean, E., Adam, P., Connan, J., Albrecht, P., 2004. Effects of weathering on nickel and vanadyl porphyrins of a Lower Toarcian shale of the Paris basin. Geochimica et Cosmochimica Acta 68, 789–804.

Hannigan, R.E., Sholkovitz, E.R., 2001. The development of middle rare earth element enrichments in freshwaters: weathering of phosphate minerals. Chemical Geology 175, 495–508.

Hatch, J.R., Leventhal, J.S., 1992. Relationship between inferred redox potential of the depositional environment and geochemistry of the Upper Pennsylvanian (Missourian) Stark Shale Member of the Dennis Limestone, Wabaunsee County, Kansas, U.S.A. Chemical Geology 99, 65–82.

Helz, G.R., Miller, C.V., Charnock, J.M., Mosselmans, J.F. W., Pattrick, R.A.D., Garner, C.D., Vaughan, D.J., 1996. Mechanism of molybdenum removal from the sea and its concentration in black shales: EXAFS evidence. Geochimica et Cosmochimica Acta 60, 3631–3642.

Huerta-Diaz, M.A., Morse, J.W., 1992. Pyritization of trace metals in anoxic marine sediments. Geochimica et Cosmochimica Acta 56, 2681–2702.

Immenhauser, A., Kenter, J.A.M., Ganssen, G., Bahamonde, J.R. Van, Vliet, A., Saher, M.H., 2002. Origin and significance of isotope shifts in Pennsylvanian carbonates (Asturias, NW Spain). Journal of Sedimentary Research 72, 82–94.

Jaffe, L.A., Peucker-Ehrenbrink, B., Petsch, S.T., 2002. Mobility of rhenium, platinum group elements and organic carbon during black shale weathering. Earth and Planetary Science Letters 198, 339–353.

Joachimski, M.M., van Geldern, R., Breisig, S., Buggisch, W., Day, J., 2004. Oxygen isotope evolution of biogenic calcite and apatite during the Middle and Late Devonian. International Journal of Earth Sciences 93, 542–553.

Jones, B., Manning, D.A.C., 1994. Comparison of geochemical indices used for the interpretation of palaeoredox conditions in ancient mudstone. Chemical Geology 111, 111–129.

Keller, P. Gehring, A., 1992. Different weathering stages indicated by the magnetization of limestones: An example from the southeast Pyrenees, Spain Earth and Planetary Science Letters 111, 49–57.

Kolowith, L.C., Berner, R.A., 2002. Weathering of phosphorus in black shales. Global Biogeochemical Cycles 16, doi: 10.1029/2001GB001887. issn: 0886–6236.

Kump, L.R., Arthur, M.A., 1999. Interpreting carbon-isotope excursions: carbonates and organic

Landais, P., Michels, R., Kister, J., Dereppe, J.-M., Benkhedda Z. 1991. Behavior of Oxidized Type II Kerogen during Artificial Maturation. Energy & Fuels 5, 860–866.

Lehmann, M.F., Bernasconi, S.M., Barbieri, A., McKenzie, J.A., 2002. Preservation of organic matter and alteration of its carbon and nitrogen isotope composition during simulated and in situ early sedimentary diagenesis. Geochimica et Cosmochimica Acta 66, 3573–3584.

Liermann, L.J., Mathur, R., Wasylenki, L.E., Nuester, J., Anbar, A.D., Brantley, S.L., 2011. Extent and isotopic composition of Fe and Mo release from two Pennsylvania shales in the presence of organic ligands and bacteria. Chemical Geology 281, 167–180.

Lev, S.M., Filer, J.K., 2004. Assessing the impact of black shale processes on REE and the U–Pb isotope system in the southern Appalachian Basin. Chemical Geology 206, 393–406.

Leythaeuser, D., 1973. Effects of weathering on organic matter in shales. Geochimica et Cosmochimica Acta 37, 113–120.

Lindgreen, H., Drits, V.A., Sakharov, B.A., Salyn, A.L., Wrang, P., Dainyak, L.G., 2000. Illite-smectite structural changes during metamorphism in black Cambrian Alum shales from the Baltic area. American Mineralogist 85, 1223–1238.

Littke, R., Klussmann, U., Krooss, B., Leythaeuser, D., 1991. Quantification of loss of calcite, pyrite, and organic matter due to weathering of Toarcian black shales and effects on kerogen and bitumen characteristics. Geochimica et Cosmochimica Acta 55, 3369–3378.

Liu, Y.-G., Miah, M.R.U., Schmitt, R.A., 1988. Cerium: a chemical tracer for paleo-oceanic redox conditions. Geochimica et Cosmochimica Acta 52, 1361–1371.

Lo, H.B., Cardott, B.J., 1995. Detection of natural weathering of Upper McAlester coal and Woodford Shale, Oklahoma, U.S.A. Organic Geochemistry 22, 73–83.

Lyons, T.W., Werne, J.P., Hollander, D.J., Murray, R.W., 2003. Contrasting sulfur geochemistry and Fe/Al and Mo/Al ratios across the last oxic-to-anoxic transition in the Cariaco Basin, Venezuela. Chemical Geology 195, 131–157.

Ma, L., Jin, L., Brantley, S.L., 2011. How mineralogy and slope aspect affect REE release and fractionation during shale weathering in the Susquehanna/Shale Hills critical zone observatory. Chemical Geology 290, 31–49.

Macko, S.A., Engel, M.H., Parker, P.L., 1993. Early Diagenesis of Organic Matter in Sediments. Assessment of Mechanisms and Preservation by the Use of Isotopic Molecular Approaches. In: Organic Geochemistry (eds. Engel, M.H., Macko, S.A.), 211–224.

Macko, S.A., Fogel, M.L., Hare, P.E., Hoering, T.C., 1987. Isotopic fractionation of nitrogen and carbon in the synthesis of amino acids by microorganisms. Chemical Geology 65, 79–92.

Marynowski, L., Filipiak, P., 2007. Water column euxinia and wildfire evidence during deposition of the Upper Famennian Hangenberg event horizon from the Holy Cross Mountains (central Poland). Geological Magazine 144, 569–595.

Marynowski, L., Narkiewicz, M., Grelowski, C., 2000. Biomarkers as environmental indicators in a carbonate complex, examples from the Middle Devonian, the Holy Cross Mountains, Poland. Sedimentary Geology 137, 187–212.

Marynowski L., Filipiak, P., Zatoń, M., 2010. Geochemical and palynological study of the Upper Famennian Dasberg event horizon from the Holy Cross Mountains (central Poland). Geological Magazine 147, 527–550.

Marynowski, L., Kurkiewicz, S., Rakociński, M., Simoneit, B.R.T., 2011a. Effects of weathering on organic matter: I. Changes in molecular composition of extractable organic compounds caused by paleoweathering of a Lower Carboniferous (Tournaisian) marine black shale. Chemical Geology 285, 144–156.

Marynowski, L., Szełęg, E., Jędrysek, M.O., Simoneit, B.R.T., 2011b. Effects of weathering on organic matter: II. Fossil wood weathering and implications for organic geochemical and petrographic studies. Organic Geochemistry 42, 1076–1088.

Marynowski, L., Zatoń, M., Rakociński, M., Filipiak, P., Kurkiewicz, S., Pearce, T.J., 2012. Deciphering the upper Famennian Hangenberg Black Shale depositional environments based on multi-proxy record. Palaeogeography, Palaeoclimatology, Palaeoecology 346/347, 66–86.

McArthur, J.M., Walsh, J.N., 1984. Rare-Earth geochemistry of phosphorites. Chemical Geology 47, 191–220.

McCarty, D.K., Theologou, P.N., Fischer, T.B., Derkowski, A., Stokes, M.R., Ollila, A., 2015. Mineral-chemistry quantification and petrophysical calibration for multimineral evaluations: A nonlinear approach. AAPG Bulletin, in press. DOI: 10.1306/01221514195

Mort, H.P., Slomp, C.P. Gustafsson, B.G., Andersen, T.J., 2010. Phosphorus recycling and burial in Baltic Sea sediments with contrasting redox conditions. Geochimica et Cosmochimica Acta 74, 1350–1362.

Möbius, J., 2013. Isotope fractionation during nitrogen remineralization (ammonification): Implications for nitrogen isotope biogeochemistry. Geochimica et Cosmochimica Acta 105, 422–432.

Morford, J.L., Emerson, S., 1999. The geochemistry of redox sensitive trace metals in sediments. Geochimica et Cosmochimica Acta 63, 1735–1750.

Nägler, T.F., Siebert, C., Lüschen, H., Böttcher, M.E., 2005. Sedimentary Mo isotope record across the Holocene fresh-brackish water transition of the Black Sea. Chem. Geol. 219, 283–295.

Obreht, I., Buggle, B., Catto, N., Marković, S.B., Bösel, S., Vandenberghe, D.A.G., Hambach, U., Svirčev, Z., Lehmkuhl, F., Basarin, B., Gavrilov, M.B., Jović, G., 2014. The Late Pleistocene Belotinac section (southern Serbia) at the southern limit of the European loess belt: Environmental and climate reconstruction using grain size and stable C and N isotopes. Quaternary International 334–335, 10–19.

Pearce, C.R., Cohen, A.S., Coe, A.L., Burton, K.W., 2008. Molybdenum isotope evidence for global ocean anoxia coupled with perturbations to the carbon cycle during the early Jurassic. Geology 36, 231–234.

Pearce, C.R., Cohen, A.S., Parkinson, I.J., 2009. Quantitative separation of molyb-denum and rhenium from geological materials for isotopic determination by MC-ICP-MS. Geostand. Geoanal. Res. 33, 219–229.

Philippsen, B., Olsen, J., Lewis, J.P., Rasmussen, P., Ryves, D.B., Knudsen, K.L., 2013. Mid- to late-Holocene reservoir-age variability and isotope-based palaeoenvironmental reconstruction in the Limfjord, Denmark. The Holocene 23, 1017–1027.

Peucker-Ehrenbrink, B., Hannigan, R. E. 2000. Effects of black shale weathering on the mobility of rhenium and platinum group elements. Geology 28, 475–478.

Perkins, R.B., Mason, Ch.E., 2015. The relative mobility of trace elements from short-term weathering of a black shale. Applied Geochemistry 56, 67–79.

Petsch, S.T., Berner, R.A., Eglinton, T.I., 2000. A field study of the chemical weathering of ancient sedimentary organic matter. Organic Geochemistry 31, 475–487.

Pollack, G.D., Krogstad, E.J., Bekker, A., 2009. U–Th–Pb–REE systematics of organic-rich shales from the ca. 2.15 Ga Sengoma Argillite Formation, Botswana: Evidence for oxidative continental weathering during the Great Oxidation Event. Chemical Geology 260, 172–185.

Pope, G.A., Dorn, R.I., Dixon, J.C., 1995. A new conceptual model for understanding geographical variations in weathering. Annals of the Association of American Geographers 85, 38–64.

Popp, B.N., Parekh, P., Tilbrook, B., Bidigare, R.R., Laws, E.A., 1997. Organic carbon $\delta^{13}C$ variations in sedimentary rocks as chemostratigraphic and paleoenvironmental tools. Palaeogeography, Palaeoclimatology, Palaeoecology 132, 119–132.

Popp, B.N., Takigiku, R., Hayes, J.M., Louda, J.W., Baker, E.W., 1989. The post-Paleozoic chronology and mechanism of 13C depletion in primary marine organic matter. American Journal of Science 289, 436–454.

Poulson, R.L., Siebert, C., McManus, J., Berelson, W.M., 2006. Authigenic molybdenum isotope signatures in marine sediments. Geology 34, 617–620.

Pujol, F., Berner, Z., Stüben, D., 2006. Palaeoenvironmental changes at the Frasnian/Famennian boundary in key European sections: chemostratigraphical constraints. Palaeogeography, Palaeoclimatology, Palaeoecology 240, 120–145.

Rachidi, M., Neuweiler, F., Kirkwood, D., 2009. Origin and diagenetic history of a Lower Jurassic petroleum source rock, Middle Atlas, Morocco. Journal of Petroleum Geology 32, 111-128.

Racka, M., Marynowski, L., Filipiak, P., Sobstel, M., Pisarzowska, A., Bond, D.P.G., 2010. Anoxic Annulata Events in the Late Famennian of the Holy Cross Mountains (Southern Poland): geochemical and palaeontological record. Palaeogeography, Palaeoclimatology, Palaeoecology 297, 549–575.

Racki, G., Racka, M., Matyja, H., Devleeschouwer, X., 2002. The Frasnian/Famennian boundary interval in the South Polish–Moravian shelf basins: integrated event stratigraphical approach. Palaeogeography, Palaeoclimatology, Palaeoecology 181, 251–297.

Racki, G., Baliński, A., Wrona, R., Małkowski, K., Drygant, D., Szaniawski, H., 2012. Faunal dynamics across the Silurian–Devonian positive isotope excursions ($\delta^{13}C$, $\delta^{18}O$) in Podolia, Ukraine: Comparative analysis of the Ireviken and Klonk events. Acta Palaeontologica Polonica 57, 795–832.

Reitz, A., Wille, M., Nägler, T.F., de Lange, G.J., 2007. Atypical Mo isotope signatures in eastern Mediterranean sediments. Chemical Geology 245, 1–8.

Rimmer, S.M., 2004. Geochemical paleoredox indicators in Devonian–Mississipian black shales, Central Appalachian Basin (USA). Chemical Geology 206, 373–391.

Rimmer, S.M., Thomson, J.A., Goodnight, S.A., Robl, T.L., 2004. Multiple controls on the preservation of organic matter in Devonian–Mississipian marine black shales: geochemical and petrographic evidence. Palaeogeography, Palaeoclimatology, Palaeoecology 215, 125–154.

Riquier, L., Tribovillard, N., Averbuch, O., Devleeschouwer, X., Riboulleau, A., 2006. The Late Frasnian Kellwasser horizons of the Harz Mountains (Germany): two oxygen-deficient periods resulting from different mechanisms. Chemical Geology 233, 137–155.

Rooney, A., Goodhue, R., Clayton, G., 2015. Stable nitrogen isotope analysis of the Upper Devonian palynomorph, Tasmanites. Palaeogeography, Palaeoclimatology, Palaeoecology 429, 13–21.

Ross, D.J.K., Bustin, R.M., 2009. Investigating the use of sedimentary geochemical proxies for paleoenvironment interpretation of thermally mature organic-rich strata: Examples from the Devonian–Mississippian shales, Western Canadian Sedimentary Basin. Chemical Geology 260, 1–19.

Rudnick, R.L., Gao S., 2003. Composition of the continental crust. In: Rudnick R.L. (ed) The crust, Treatise on Geochemistry, vol 3. Elsevier, Oxford, pp. 1–70.

Sachs, J., Repeta, D., 1999. Oligotrophy and nitrogen fixation during eastern Mediteranean sapropel events. Science 286, 2485–2488.

Sackett, W.M., Thompson, R.R., 1963. Isotope organic carbon composition of Recent continental derived clastic sediments of Eastern Gulf Coast, Gulf of Mexico, Am. Assoc. Petrol. Geol. 147, 535–531.

Saino T., 1992. ^{15}N and ^{13}C natural abundance in suspended particulate organic matter from a Kuroshio warm-core ring. Deep-Sea Research 39, 5317–5362.

Schmitz, B., Charisi, S.D., Thompson, E.I., Speijer, R.P., 1997. Barium, SiO_2 (excess), and P_2O_5 as proxies of biological productivity in the Middle East during the Palaeocene and the latest Palaeocene benthic extinction event. Terra Nova 9, 95–99.

Schoepfer, S.D., Shen, J., Wei, H., Tyson, R.H., Ingall, E., Algeo, T.J., 2014. Total organic carbon, organic phosphorus, and biogenic barium fluxes as proxies for paleomarine productivity. Earth-Science Reviews (in press, doi:10.1016/j.earscirev.2014.08.017)

Siebert, C., Nägler, T.F., von Blanckenburg, F., Kramers, J.D., 2003. Molybdenum isotope record as a potential new proxy for paleoceanography. Earth Planet. Sci. Lett. 211, 159–171.

Siebert, C., McManus, J., Bice, A., Poulson, R., Berelson,W.M., 2006. Molybdenum isotope signatures in continental margin marine sediments. Earth Planet. Sci. Lett. 241, 723–733.

Slomp, C.P., Van Der Gaast, S.J., Van Raaphorst, W., 1996. Phosphorus binding by poorly crystalline iron oxides in North Sea sediments. Marine Chemistry 52, 55–73.

Szaniawski, R., 2008. Late Paleozoic geodynamics of the Malopolska Massif in the light of new paleomagnetic data for the southern Holy Cross Mountains. Acta Geologica Polonica 58, 1–12.

Szaniawski, R., Konon, A., Grabowski, J., Schnabl, P., 2011. Palaeomagnetic age constraints on folding and faulting events in Devonian carbonates of the Kielce Fold Zone (southern Holy Cross Mountains, Central Poland). Geological Quarterly 55, 223–234.

Szulczewski, M., 1995. Depositional evolution of the Holy Cross Mts. (Poland) in the Devonian and Carboniferous - a review. Geological Quarterly 39, 471–488.

Śliwiński, M.G., Whalen, M.T., Newberry, R.J., Payne, J.H., Day, J.E., 2011. Stable isotope ($\delta^{13}C_{carb}$ and org, $\delta^{15}N_{org}$) and trace element anomalies during the Late Devonian 'punctata Event' in the Western Canada Sedimentary Basin. Palaeogeography, Palaeoclimatology, Palaeoecology 307, 245–271.

Środoń, J., Paszkowski, M., 2011. Role of clays in diagenetic history of boron and nitrogen in the Carboniferous of Donbas (Ukraine). Clay Minerals 46, 561–582.

Środoń, J., Szulc, J., Anczkiewicz, A., Jewuła, K., Banaś, M., Marynowski, L., 2014. Weathering, sedimentary and diagenetic controls of mineral and geochemical characteristics of the vertebrate-bearing Silesian Keuper. Clay Minerals 49, 569–594.

Tamamura, S., Ueno, A., Aramaki, N., Matsumoto, H., Uchida, K., Igarashi, T., Kaneko, K., 2015. Effects of oxidative weathering on the composition of organic matter in coal and sedimentary rock. Organic Geochemistry 81, 8–19.

Torsvik, T. H., van der Voo, R., Preeden, U., Mac Niocaill, C., Steinberger, B., Doubrovine, P. V., van Hinsbergen, D. J. J., Domeier, M., Gaina, C., Tohver, E., Meert, J. G., McCausland, P. J. A., Cocks, L. R. M., 2012. Phanerozoic polar wander, paleogeography and dynamics. Earth-Science Reviews 114, 325–368.

Tribovillard, N., Algeo, T.J., Lyons, T., Riboulleau, A., 2006. Trace metals as paleoredox and paleoproductivity proxies: an update. Chemical Geology 232, 12–32.

Tribovillard, N., Algeo, T.J., Baudin, F., Riboulleau, A., 2012. Analysis of marine environmental conditions based on molybdenum-uranium covariation – Applications to Mesozoic paleoceanography. Chemical Geology 324–325, 46–58.

Tulipani, S., Grice, K., Greenwood, P.F., Haines, P.W., Sauer, P.E., Schimmelmann, A., Summons, R.E., Foster, C.B., Böttcher, M.E., Playton, T., Schwark, L., 2015. Changes of palaeoenvironmental conditions recorded in Late Devonian reef systems from the Canning Basin, Western Australia: A biomarker and stable isotope approach. Gondwana Research 28, 1500–1515.

Tuttle, M.L.W., Breit, G.N., Goldhaber, M.B., 2009. Weathering of the New Albany Shale, Kentucky: II. Redistribution of minor and trace elements. Applied Geochemistry 24, 1565–1578.

Wignall, P. B., 1994. Black shales. Oxford: Clarendon Press, 127 pp.

Wildman, R.A., Berner, R.A., Petsch, S.T., Bolton, E.W., Eckert, J.O., Mok, U., Evans, J.B., 2004. The weathering of sedimentary organic matter as a control on atmospheric O2: I. Analysis of black shale. American Journal of Science 304, 234–249.

Williams, E.L., Szramek, K., Jin, L., Ku, T.C.W., Walter, L.M., 2007. The carbonate system geochemistry of shallow groundwater/surface water systems in temperate glaciated watersheds (Michigan, USA): significance of open system dolomite weathering. Geological Society of American Bulletin 119, 515–528.

Yu, Ch., Lavergren, U., Peltola, P., Drake, H., Bergbäck, B., Åström, M.E., 2014. Retention and transport of arsenic, uranium and nickel in a black shale setting revealed by a long-term humidity cell test and sequential chemical extractions. Chemical Geology 363, 134–144.

Zwing, A., 2003. Causes and Mechanisms of Remagnetisation Palaeozoic Sedimentary Rocks a Multidisciplinary Approach. PhD thesis, LMU Munchen, (http://edoc.ub.uni-muenchen.de/archive/00001578/)

Figure caption

Fig. 1. A. Schematic geological map of the western and central part of the Holy Cross Mountains, which shows the location of the Kowala Quarry (B) and the studied outcrop with the sampling locations (C).

Fig. 2. Typical results of the thermal demagnetization of a composite three-axis IRM (A). Representative hysteresis loop after correcting for para- and diamagnetic contributions (B).

Demagnetization results of a representative specimen before tectonic correction (C). VGP results (orange - before tectonic correction; green - after tectonic correction) plotted on a synthetic APWP diagram for Baltica after Torsvik et al. (2012) (D).

Fig. 3. Composite depth plot of the KQ136 black shale that shows the trace metal ratios, Mo concentrations and stable isotope values.

Fig. 4. TOC–TS–Fe ternary diagram for the KQ136 black shale that shows significant differences from weathering. Almost all the samples from the weathering zone were located at one point because of their very low TOC values and null TS.

Fig. 5. Changes in the OM pyrolysis (Rock Eval) parameters S2 and S3 along the weathering transect.

Fig. 6. U–EF vs. Mo–EF for unweathered and two partially weathered shale samples (plot according to Algeo and Tribovillard, 2009 and Tribovillard et al., 2012 with a logarithmic scale) (A) U–EF vs.Mo–EF for all the studied samples that shows their alteration during weathering (no logarithmic scale) (B).

Fig. 7. Rare-earth element distribution patterns for the three weathering zones when normalized to PAAS (Post-Archaean Australian Shale).

Fig. 8. Composite depth plot of the KQ136 black shale that shows selected trace metal ratios vs. aluminium. The enrichment zone is highlighted in the upper partially weathered shale section.

Fig. 9. Compilation of the $\delta^{13}C_{ORG\ and\ CARB}$, $\delta^{15}N$, $\delta^{18}O_{CARB}$ and $\delta^{98}Mo$ changes across the KQ136 black shale's weathering zones.

Table captions

Table 1. Estimated palaeoenvironmental proxies and DOP values from the TOC-TS-Fe diagram for the individual zones in the KQ 136 black shale. A to F = unweathered zone, G to K = partially weathered zone, L to T = weathered zone

Table 2. Results of partitioning trace elements and REEs between the immobile and mobile rock compounds.

Table 3. Isotope results. The $\delta^{98}Mo$ is expressed relative to each laboratory's respective in-house standard. [a] The measurements were conducted at IGS PAS [b] at The Open University.

Supporting information

Fig. S1. XRD patterns of the bulk rock samples in the low-angle 2ΘKα range characteristic for clay minerals. The peak at ~4.5 Å represents the major *020* reflection of the illite+smectite group. The 10.0 Å and 5.0 Å peaks correspond to mica, while the 10-13 Å range represents illite-smectite. The 14.3 Å and 7.1 Å peaks belong to chlorite while the 14.6 Å peak corresponds to vermiculite. The peak at ~4.25 Å corresponds to quartz.

Fig. S2. XRD patterns of oriented preparations from 0.2-2 μm fractions of (A) unweathered black shale, and (B) weathered red shale. R1 – ordered illite-smectite, I – discrete illite, Q – quartz. The reflections of chlorite and vermiculitic minerals, and the low-angle reflection of illite-smectite are marked with their d values in Å. Observe the lack of swelling of chlorite after glycolation and the swelling of the vermiculitic minerals, which completely collapses to 10 Å after heating at 500°C.

Fig. S3. Composite depth plot of the KQ136 black shale that shows the major element ratios.

Fig. S4. Rock Eval pyrolysis data on a conventional OM origin and maturation van Krevelen diagram. The arrow indicates the direction of alteration from the unweathered to the partially weathered zone. The samples from the weathered zone were not analysed because of the excesively low TOC content.

Fig. S5. Th/U vs. Ni/Co (A) and V/Cr vs Ni/Co plots (B) which show the inferred redox fields (from Hartkopf-Fröder et al., 2007).

Fig. S6. Composite depth plot of the KQ136 black shale that shows the REE distribution.

Table S1. Total organic carbon, total sulphur and selected major and trace element contents in the KQ136 black shale. A to F = unweathered zone, G to K = partially weathered zone, L to T = weathered zone.

Table S2. Rare earth element (REE) concentrations (ppm) for the individual zones in the KQ 136 black shale. A to F = unweathered zone, G to K = partially weathered zone, L to T = weathered zone

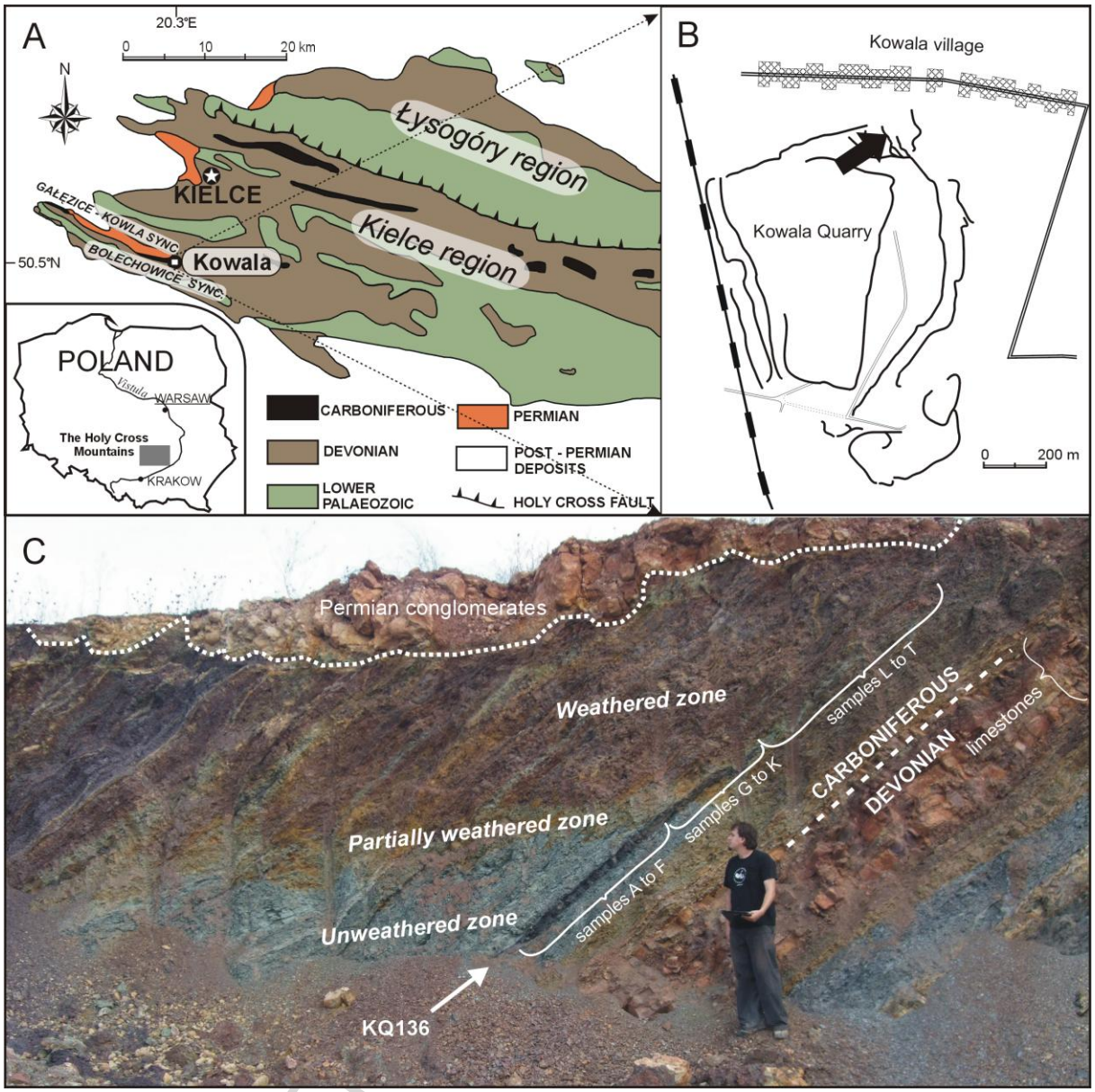

Fig. 1

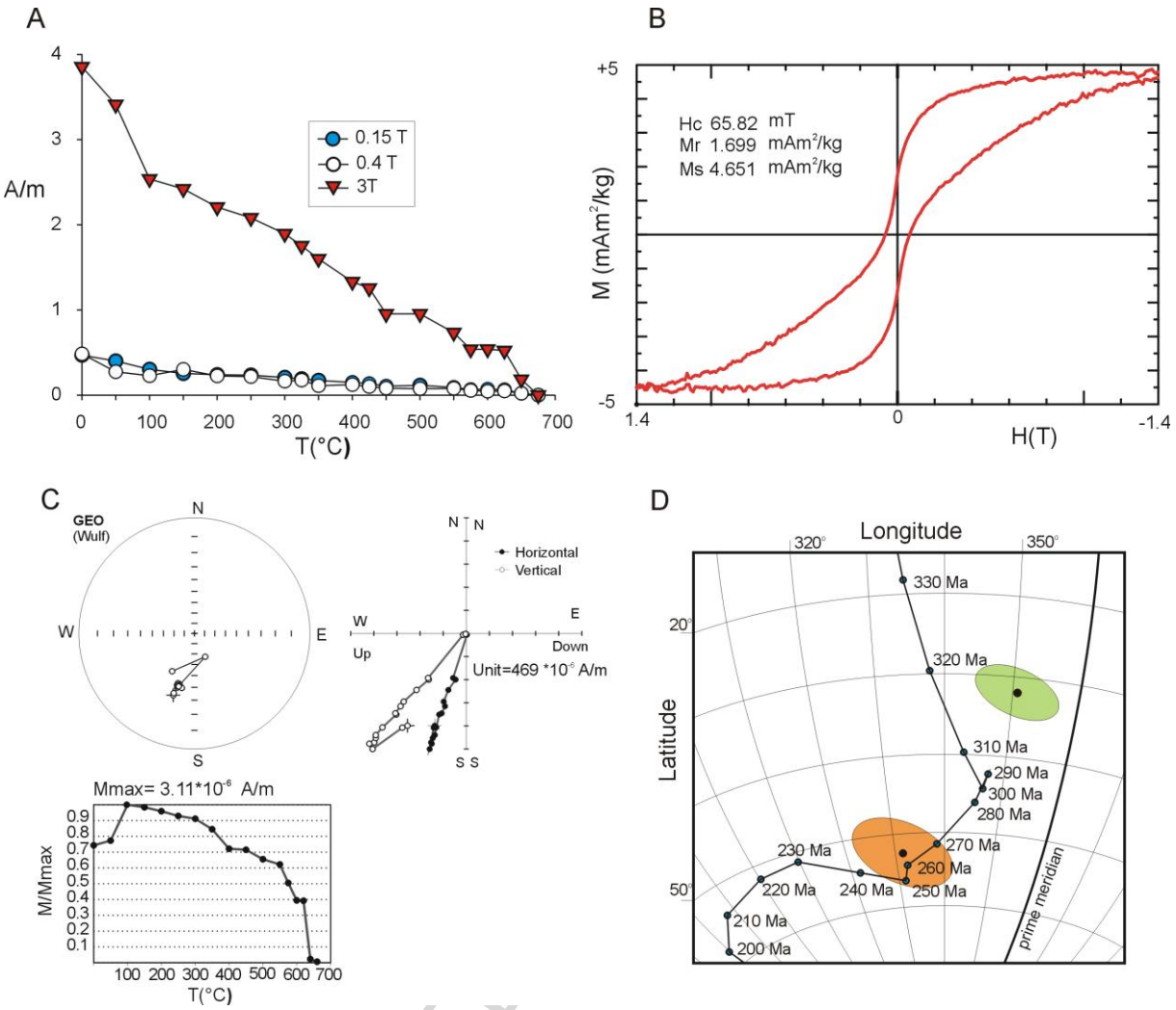

Fig. 2

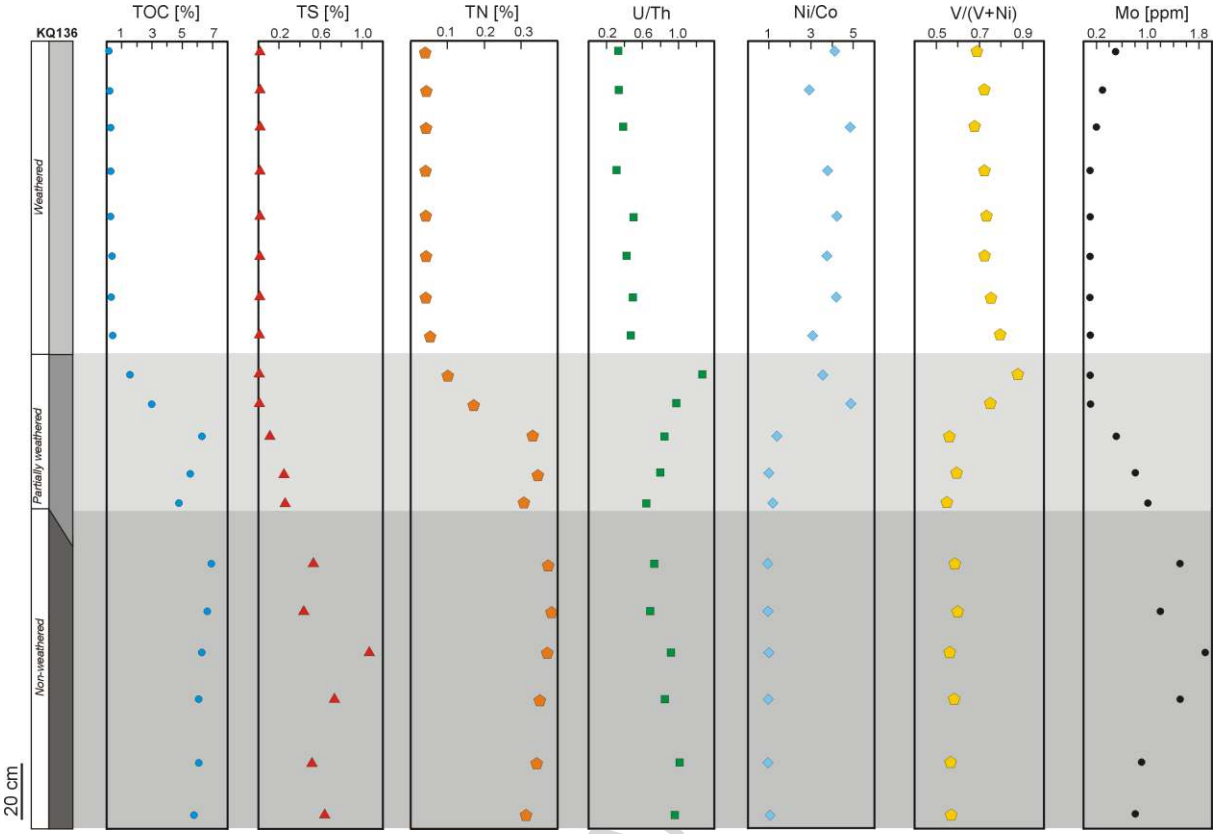

Fig. 3

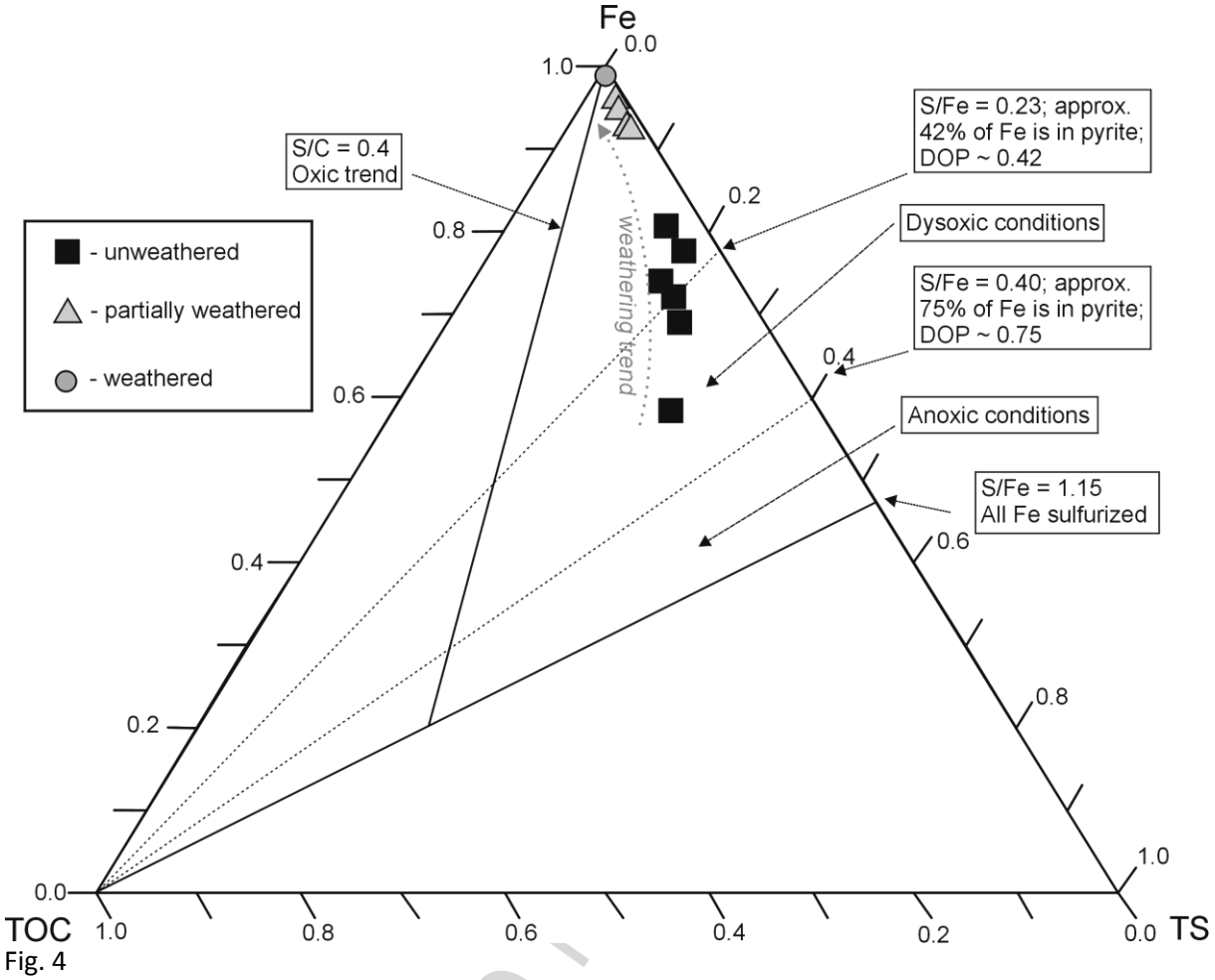

Fig. 4

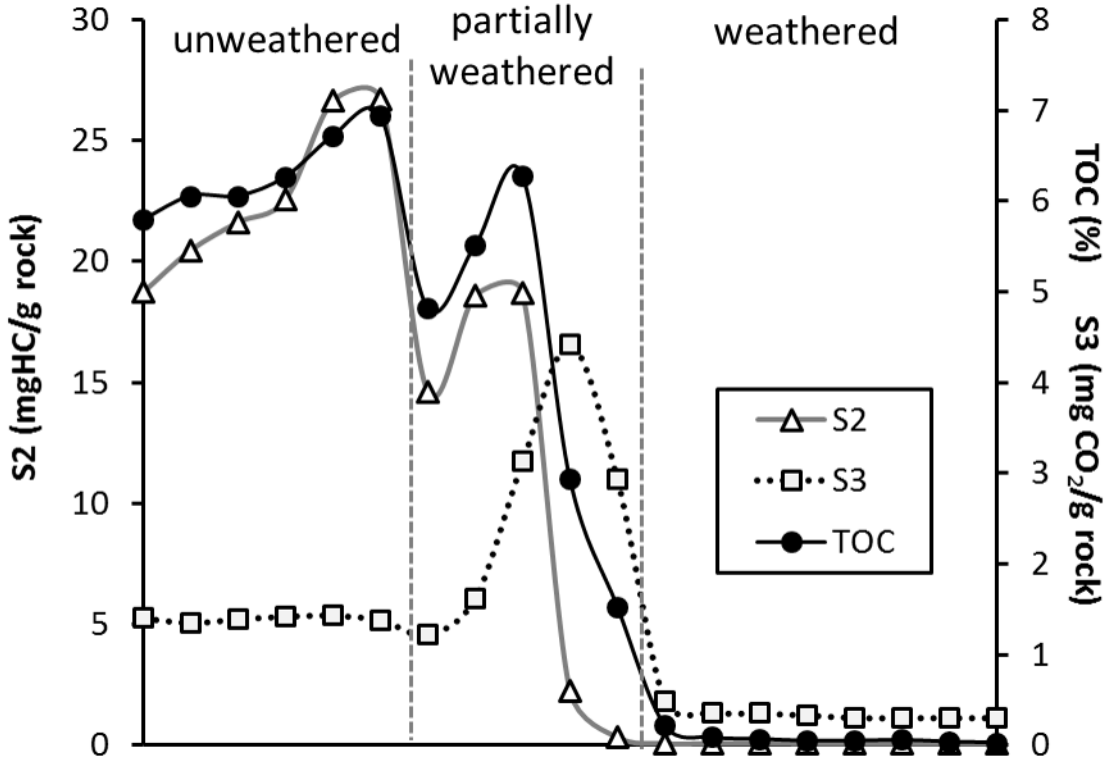

Fig. 5

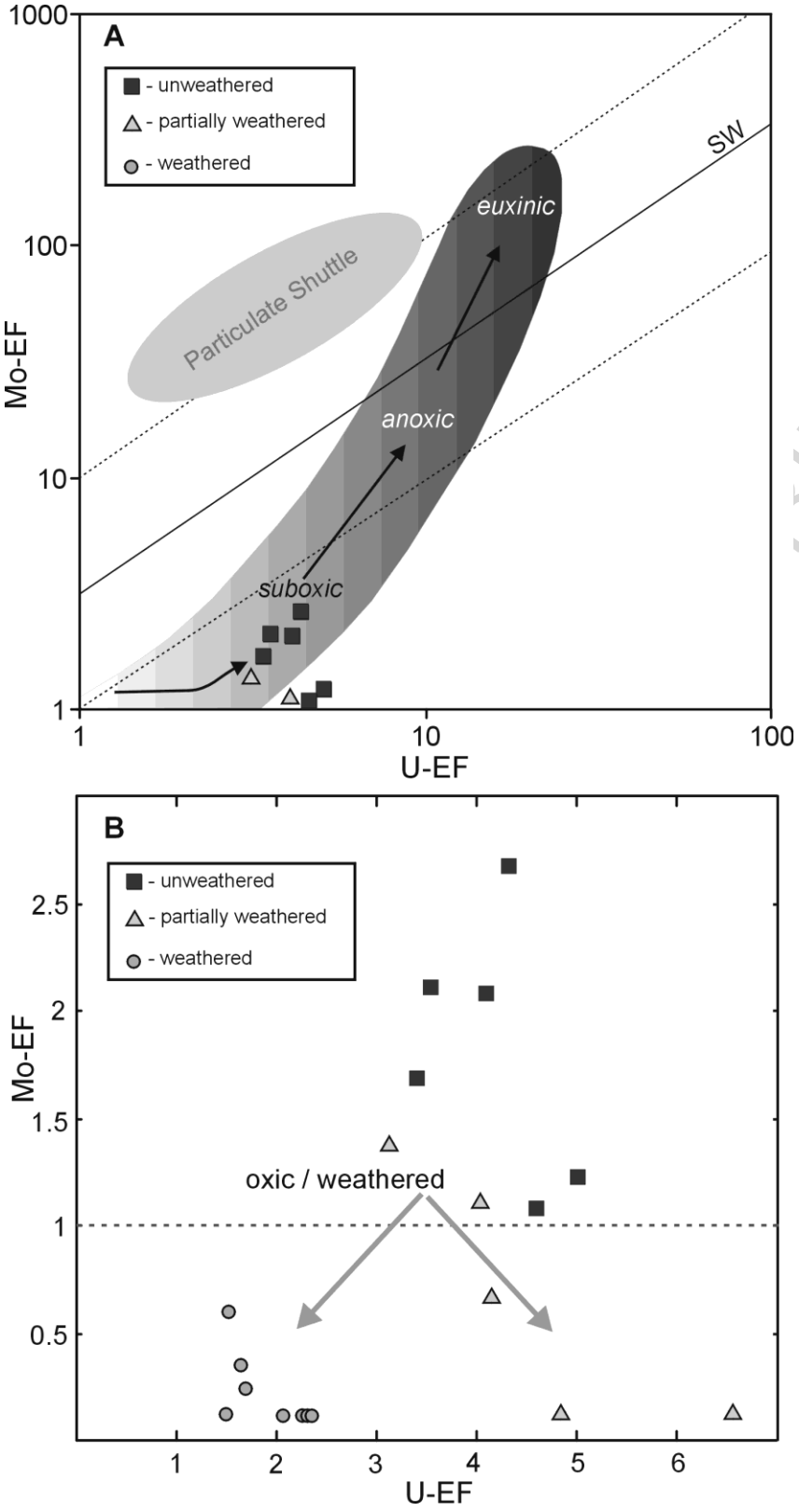

Fig. 6

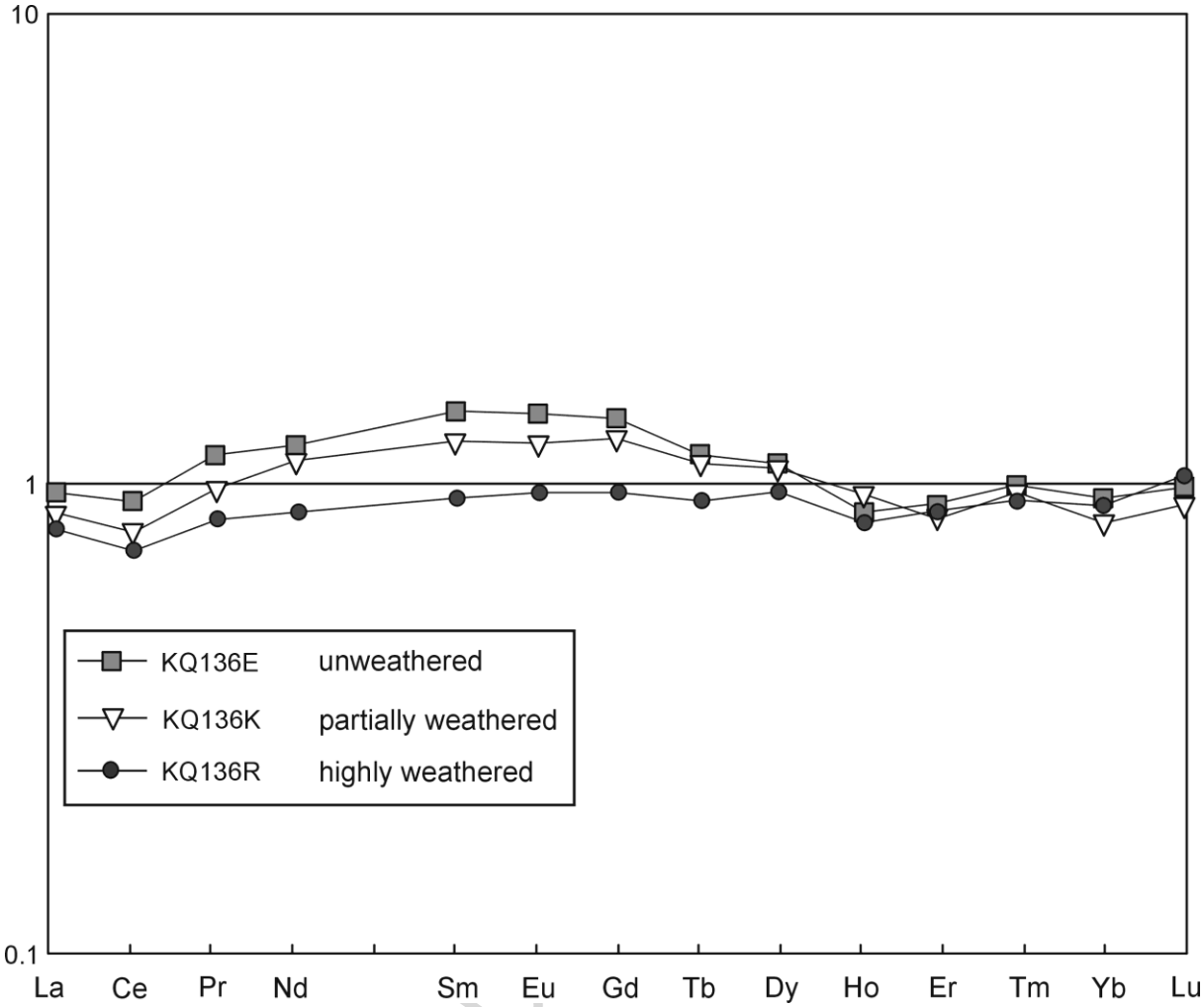

Fig. 7

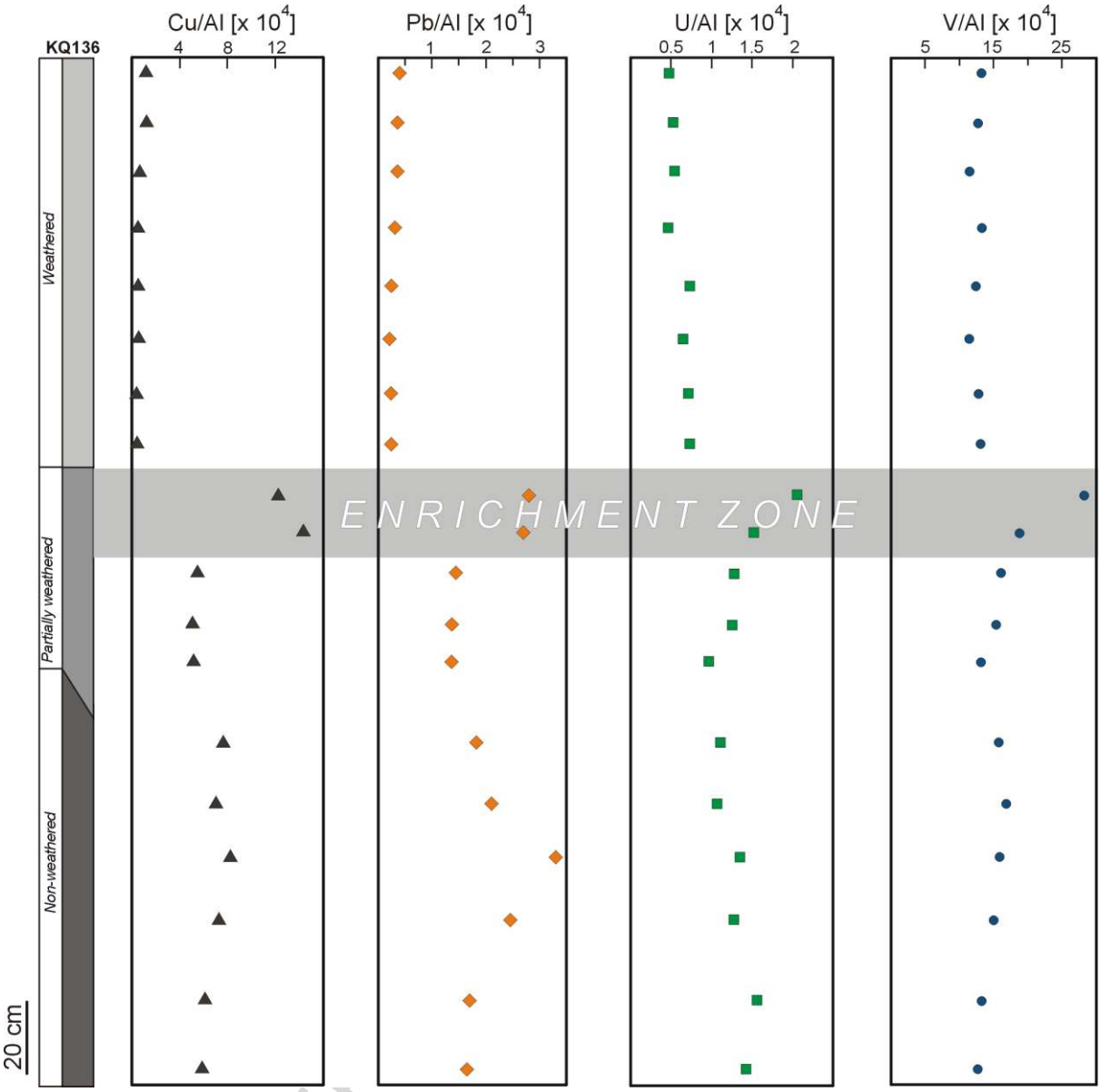

Fig. 8

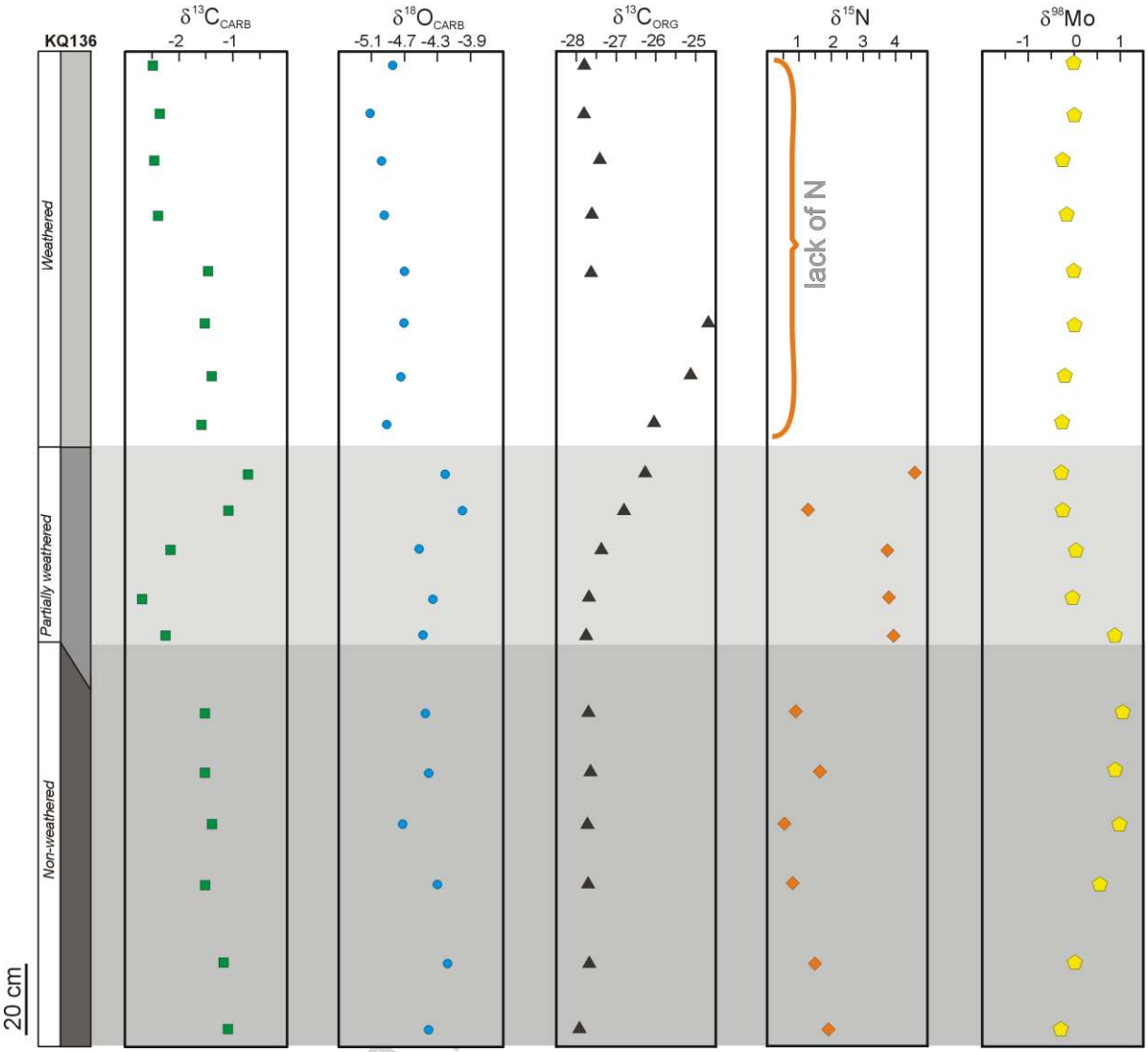

Fig. 9

Table 1. Estimated palaeoenvironmental proxies and DOP values from the TOC-TS-Fe diagram for the individual zones in the KQ 136 black shale. A to F = unweathered zone, G to K = partially weathered zone, L to T = weathered zone

Sample	Redox conditions									Productivity					
	TOC	TS	U/Th	Ni/Co	V/(V+Ni)	V/Cr	U_{auth}	Mo/TOC	Corg/P	P/Al	Ba/Al[a]	TOC/Al	Ni/Al[a]	Zn/Al[a]	C
136A	5.80	0.63	0.95	1.06	0.57	1.49	6.83	0.14	189.8	0.0041	23.84	0.79	9.51	3.93	
136B	6.06	0.51	1.01	0.97	0.57	1.42	7.63	0.15	173.7	0.0047	25.85	0.82	9.93	3.95	
136C	6.06	0.73	0.84	0.97	0.58	1.58	5.57	0.25	198.3	0.0042	23.91	0.84	10.67	4.70	
136D	6.27	1.07	0.92	0.99	0.56	1.49	6.07	0.30	179.5	0.0049	23.97	0.88	12.42	4.79	
136E	6.72	0.43	0.68	0.92	0.60	1.74	3.83	0.18	154.0	0.0061	24.60	0.94	11.25	4.64	
136F	6.95	0.52	0.73	0.92	0.59	1.64	4.23	0.22	198.9	0.0049	22.81	0.98	11.11	4.93	
136G	4.82	0.24	0.63	1.13	0.55	1.54	3.33	0.21	184.0	0.0036	24.34	0.66	10.77	5.47	
136H	5.51	0.23	0.81	1.00	0.59	1.62	5.33	0.15	180.3	0.0042	25.20	0.76	10.59	5.23	
136I	6.28	0.10	0.84	1.37	0.56	1.59	5.83	0.08	205.5	0.0041	26.54	0.83	12.65	6.37	
136J	2.94	0.001	0.98	4.89	0.74	1.99	7.93	0.03	74.8	0.0049	26.76	0.37	6.48	7.00	1
136K	1.53	0.001	1.27	3.54	0.88	2.96	11.87	0.07	43.8	0.0044	25.93	0.19	3.67	8.22	1
136L	0.33	0.0004	0.46	3.03	0.80	1.41	1.67	0.30	9.49	0.0043	25.63	0.04	3.31	7.36	
136M	0.25	0.0001	0.49	4.16	0.76	1.37	1.87	0.41	8.05	0.0037	24.21	0.03	4.05	8.27	
136N	0.23	0.0017	0.41	3.76	0.72	1.25	0.97	0.43	7.67	0.0037	24.77	0.03	4.41	8.58	
136O	0.16	0.0004	0.50	4.19	0.74	1.30	1.90	0.61	4.19	0.0049	25.46	0.02	4.39	8.61	
136P	0.23	0.0006	0.31	3.77	0.72	1.32	-0.33	0.44	7.43	0.0037	25.15	0.03	5.09	9.72	
136R	0.21	0.0010	0.37	4.80	0.68	1.24	0.47	0.97	6.72	0.0037	23.01	0.02	5.32	10.35	
136S	0.16	0.0011	0.34	2.92	0.72	1.37	0.03	1.90	4.03	0.0048	24.53	0.02	4.97	10.93	
136T	0.05	0.0016	0.33	4.06	0.69	1.43	-0.10	10.93	1.31	0.0043	24.23	0.01	5.93	13.51	

[a] – ratio values multiplied 10^4 times

$U_{auth} = U_{total} – Th_{total}/3$

Table 2. Results of partitioning trace elements and REEs between the immobile and mobile rock compounds.

Element	Ba	Sr	Cu	U	V	Pb	Co	Ni	Cr	Mo	Zn
Immobile compound (Al) coefficient, C_{IM}	24.16	5.52	0.18	0.60	11.62	0.35	0.72	4.41	9.28	0.03	1.11
Best contributing mobile compound	RE-S3	TIC	RE-S3	RE-S3	RE-S3	RE-S3	TOC	TOC	Total-S	Total-S	Fe
Mobile compound coefficient, C_{MOB}	3.94	64.27	25.87	2.46	18.35	5.38	11.60	7.72	2.92	1.71	16.64
Mobile/immobile coefficients ratio C_{MOB} / C_{IM}	0.163	11.6	145	4.1	1.58	15.3	16.1	1.75	0.31	61.4	14.9

Element	La	Ce	Pr	Nd	Sm	Eu	Gd	Tb	Dy	Ho	Er	Tm	Yb	Lu
Immobile compound (Al) coefficient, C_{IM}	3.795	7.307	0.977	3.662	0.732	0.138	0.620	0.098	0.561	No valid model found		0.046	0.300	0.048
Best contributing mobile compound	TOC	TOC	TOC	TOC	TOC	TOC	TOC	TOC	TOC			TIC	TIC	TOC
Mobile compound coefficient, C_{MOB}	1.310	2.409	0.362	1.444	0.265	0.055	0.255	0.030	0.142			0.030	0.228	0.005
Mobile/immobile	0.345	0.330	0.370	0.394	0.363	0.398	0.411	0.306	0.253			0.664	0.760	0.098

coefficients ratio C_{MOB} / C_{IM}													

Table 3. Isotope results. The δ^{98}Mo is expressed relative to each laboratory's respective in-house standard. [a] The measurements were conducted at IGS PAS [b] at The Open University.

Sample	$\delta^{13}C_{org}$ (‰)	$\delta^{15}N$ (‰)	$\delta^{13}C_{carb}$ (‰)	$\delta^{18}O_{carb}$ (‰)	$\delta^{98/95}$Mo (‰)[a]	External reproducibility (2 S.D. ‰)[a]	$\delta^{98/95}$Mo (‰)[b]	External reproducibility (2 S.D. ‰)[b]
KQ136A	-27.92	1.95	-1.09	-4.40	-0.32	0.16	-0.34	0.20
KQ136B	-27.67	1.48	-1.17	-4.17	0.00	0.21		
KQ136C	-27.71	0.81	-1.50	-4.30	0.53	0.26		
KQ136D	-27.70	0.52	-1.39	-4.71	0.93	0.16		
KQ136E	-27.63	1.61	-1.52	-4.40	0.91	0.38		
KQ136F	-27.71	0.89	-1.50	-4.44	1.15	0.22	1.02	0.20
KQ136G	-27.75	3.95	-2.25	-4.46	0.90	0.23		
KQ136H	-27.68	3.74	-2.64	-4.35	-0.05	0.26	0.08	0.05
KQ136I	-27.42	3.68	-2.14	-4.52	0.11	0.06		
KQ136J	-26.81	1.25	-1.06	-3.99	-0.24	0.10		
KQ136K	-26.30	4.61	-0.70	-4.20	-0.32	0.22	-0.36	0.20
KQ136L	-26.06		-1.56	-4.91	-0.30	0.10		
KQ136M	-25.12		-1.39	-4.73	-0.24	0.07		
KQ136N	-24.70		-1.51	-4.70	-0.01	0.14	0.18	0.20
KQ136O	-27.62		-1.45	-4.69	0.04	0.19		
KQ136P	-27.60		-2.40	-4.94	-0.17	0.20		
KQ136R	-27.42		-2.45	-4.98	-0.28	0.20		
KQ136S	-27.83		-2.35	-5.10	0.02	0.20	0.05	0.05
KQ136T	-27.82		-2.48	-4.84	-0.07	0.20		

Highlights

1. Permian weathering of black shale took place at dry climate
2. Palaeoenvironmental geochemical proxies, such as U/Th, Ni/Co, Mo have been altered by weathering
3. Elements bound to iron sulphides are especially prone to be removed from weathered black shale
4. Weathering caused significant changes of the C, O, N and Mo stable isotope compositions